Novel role of neuronal Ca^{2+} sensor-1 as a survival factor up-regulated in injured neurons

Tomoe Y. Nakamura,[1,2] Andreas Jeromin,[4] George Smith,[5] Hideaki Kurushima,[3] Hitoshi Koga,[2] Yusaku Nakabeppu,[3] Shigeo Wakabayashi,[1] and Junichi Nabekura[2,6,7]

[1]Department of Molecular Physiology, National Cardiovascular Center Research Institute, Suita, Osaka 565-8565, Japan
[2]Department of Cellular and System Physiology, Graduate School of Medical Sciences and [3]Division of Neurofunctional Genomics, Department of Immunobiology and Neuroscience, Medical Institute of Bioregulation, Kyushu University, Fukuoka 812-8582, Japan
[4]Neuroscience, Baylor College of Medicine, Houston, TX 77030
[5]Department of Physiology, University of Kentucky Medical School, Lexington, KY 50536
[6]Division of Homeostatic Development, National Institute of Physiological Sciences, Okazaki 444-8585, Japan
[7]Core Research for Evolutional Science and Technology, the Japan Science and Technology Agency, Kawaguchi, Saitama 332-0012, Japan

A molecular basis of survival from neuronal injury is essential for the development of therapeutic strategy to remedy neurodegenerative disorders. In this study, we demonstrate that an EF-hand Ca^{2+}-binding protein neuronal Ca^{2+} sensor-1 (NCS-1), one of the key proteins for various neuronal functions, also acts as an important survival factor. Overexpression of NCS-1 rendered cultured neurons more tolerant to cell death caused by several kinds of stressors, whereas the dominant-negative mutant (E120Q) accelerated it. In addition, NCS-1 proteins increased upon treatment with glial cell line–derived neurotrophic factor (GDNF) and mediated GDNF survival signal in an Akt (but not MAPK)-dependent manner. Furthermore, NCS-1 is significantly up-regulated in response to axotomy-induced injury in the dorsal motor nucleus of the vagus neurons of adult rats in vivo, and adenoviral overexpression of E120Q resulted in a significant loss of surviving neurons, suggesting that NCS-1 is involved in an antiapoptotic mechanism in adult motor neurons. We propose that NCS-1 is a novel survival-promoting factor up-regulated in injured neurons that mediates the GDNF survival signal via the phosphatidylinositol 3-kinase–Akt pathway.

Introduction

Neuronal apoptosis is induced by numerous stressors and underlies many human neurodegenerative disorders, such as Alzheimer's and Parkinson's disease. Under such apoptotic conditions, several neurotrophic factors such as glial cell line–derived neurotrophic factor (GDNF) and brain-derived neurotrophic factor (BDNF) can activate the antiapoptotic process to rescue neurons from death. However, the signaling pathway leading to cell survival is not yet completely understood. GDNF was reported to exert a potent survival-promoting activity in neurons (Henderson et al., 1994; Oppenheim et al., 1995; Yan et al., 1995) and to reduce neuronal death induced by various toxic challenges both in vitro (Nicole et al., 2001) and in vivo (Wang et al., 2002; Kirik et al., 2004). Recent evidence suggests that a part of molecular mechanisms for GDNF-induced cell survival relates to an increase in intracellular Ca^{2+} concentration, and it subsequently activates some survival pathways such as the phosphatidylinositol 3-kinase (PI3-K)–Akt pathway (Perez-Garcia et al., 2004).

Ca^{2+} is the most versatile and important intracellular messenger in neurons, regulating a variety of neuronal processes such as neurotransmission and signal transductions. The various actions of Ca^{2+} are mediated by a large family of EF-hand Ca^{2+}-binding proteins, which may act as Ca^{2+} sensors or Ca^{2+} buffers. One of them, neuronal Ca^{2+} sensor-1 (NCS-1; mammalian homologue of frequenin), was originally identified in *Drosophila melanogaster* in a screen for neuronal hyperexcitability mutants (Mallart et al., 1991). Overexpression of NCS-1 has been shown to enhance evoked neurotransmitter release and exocytosis (Pongs et al., 1993; Olafsson et al., 1995). NCS-1 directly interacts with phosphatidylinositol 4-hydroxykinase (PI4-K; Hendricks et al., 1999; Weisz et al., 2000) and enhances neuronal secretion by modulating vesicular trafficking steps in

Correspondence to Tomoe Y. Nakamura: tomoen@ri.ncvc.go.jp

Abbreviations used in this paper: BDNF, brain-derived neurotrophic factor; DMV, dorsal motor nucleus of the vagus; GAPDH, glyceraldehyde-3-phosphate dehydrogenase; GDNF, glial cell line–derived neurotrophic factor; MEK, MAPK kinase; NCS-1, neuronal Ca^{2+} sensor-1; PH, pleckstrin homology; PI3-K, phosphatidylinositol 3-kinase; PI4-K, phosphatidylinositol 4-hydroxykinase.

The Journal of Cell Biology, Vol. 172, No. 7, March 27, 2006 1081–1091
http://www.jcb.org/cgi/doi/10.1083/jcb.200508156

a phosphoinositide-dependent manner (Koizumi et al., 2002). We have previously demonstrated that NCS-1 modulates the voltage-gated K^+ channel Kv4 (Nakamura et al., 2001). Subsequently, certain voltage-gated Ca^{2+} channels have also been reported to be regulated by NCS-1 (Weiss et al., 2000; Wang et al., 2001; Tsujimoto et al., 2002). Furthermore, NCS-1 enhances the number of functional synapses (Chen et al., 2001), potentiates paired pulse facilitation (Sippy et al., 2003), and may be involved in associative learning and memory in *Caenorhabditis elegans* (Gomez et al., 2001). Despite the participation of NCS-1 in a wide range of biological functions, however, the role of NCS-1 in neuronal survival under pathophysiological conditions or the involvement of NCS-1 in neurotrophic factor–mediated neuroprotection are unknown.

Because we found that the expression levels of NCS-1 is significantly higher in immature brain (Nakamura et al., 2003) and a remarkable similarity exists between immature and injured neurons during the development and regeneration process, respectively (Nabekura et al., 2002b), these findings prompted us to study the expression level and the functional roles of NCS-1 in damaged neurons.

In this study, we found that NCS-1 is a survival-promoting factor, which increases the resistance of neurons to several kinds of stressors. In addition, NCS-1 is up-regulated in response to axonal injury in adult motor neurons, and this protects cells from apoptosis. Furthermore, NCS-1 mediates GDNF-induced neuroprotection via activation of Akt pathways. This is the first study demonstrating a novel role of NCS-1 on neuronal survival.

Results

The expression level of NCS-1 protein increases with neuronal injury

To examine the expression level of NCS-1 in injured neurons, we performed unilateral vagal axotomy (transaction of nerves) on adult rats. 1 d to 2 mo after the in vivo axotomy, brainstems, including the bilateral dorsal motor nucleus of the vagus (DMV) neurons, were isolated. Immunohistochemical staining and computerized image analysis of frozen sections revealed that axotomy significantly (more than threefold) increased the expression level of NCS-1 in the DMV when compared with those on the control side at 1 wk after the surgery (Fig. 1, A–C). NCS-1 immunoreactivity was mainly expressed in cell bodies of neurons, as shown using hematoxylin counterstaining to identify the nuclei (Fig. 1 B, brown staining accompanied with blue staining; depicted by arrows). The increase in NCS-1 level started at 1 d after axotomy, reached a peak at 1 wk, and gradually decreased to control levels over the next 2 mo (Fig. 1 D). We also conducted quantitative immunoblot analysis on tissue samples from DMV neurons 1 d and 1 wk after axotomy, expressing NCS-1 density relative to levels of glyceraldehyde-3-phosphate dehydrogenase (GAPDH). The results confirmed the immunohistochemistry experiments, with levels of NCS-1 protein in ipsilateral DMV being increased significantly (by about threefold) by 1 wk after axotomy (Fig. 1, E and F).

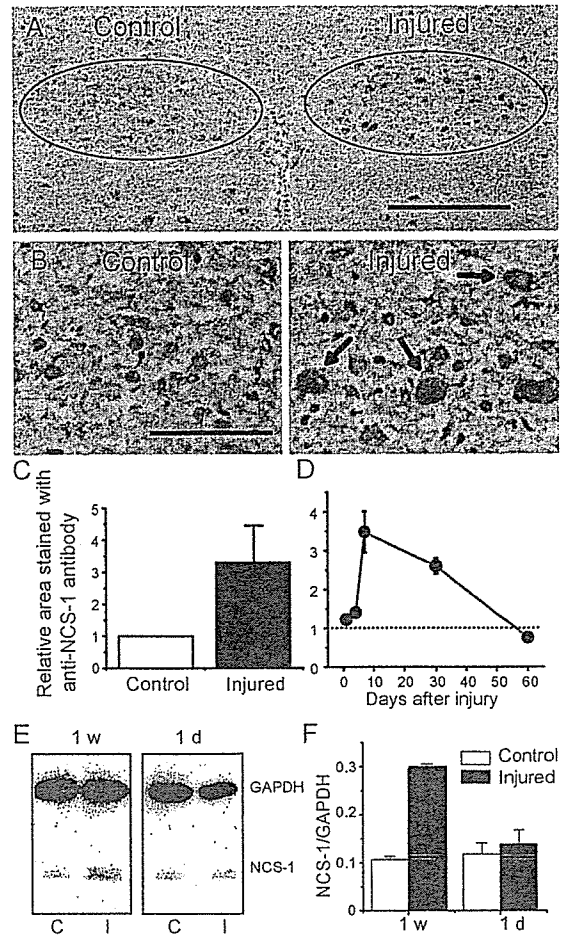

Figure 1. **NCS-1 is up-regulated in the DMV neurons after in vivo axotomy.** The 10th cranial nerve on one side of the neck of adult (4–6-wk-old) rats was cut, and, 1 d to 2 mo later, the brainstem was excised and frozen sections were cut. The NCS-1 expression was examined by counterstaining with NCS-1 antibody (brown signal) and with hematoxylin to identify nuclei (blue signal). (A) Staining pattern 1 wk after in vivo axotomy. The amount of NCS-1 protein increased in the DMV neurons ipsilateral to axotomy (injured side) when compared with control neurons contralateral to axotomy. Positions of DMV neurons are represented by circles. (B) Magnified image of DMV neurons. Arrows indicate that some neurons have both NCS-1 and hematoxylin staining, indicating that NCS-1 is expressed in cell bodies. Bars (A), 200 μm; (B) 50 μm. (C) Summarized data obtained by computerized image analysis. The relative area stained using NCS-1 antibody on the injured side 1 wk after axotomy was normalized to that of the control side (means ± SEM [error bars]; $n = 6$). (D) Time course of the expression levels of NCS-1 in injured DMV neurons relative to uninjured DMV neurons. Immunohistochemical analysis of NCS-1 levels were performed in rats 1, 4, 7, 30, and 60 d after axotomy (means ± SEM; $n = 6$). (E) Immunoblots indicating the expression levels of NCS-1 in the tissue samples obtained from DMV regions in brainstem sections at control (C) and injured sites (I) 1 wk and 1 d after axotomy. 10 sections were used for each group. Similar amount of proteins were loaded on the gel as indicated by the similar amount of the internal control GAPDH. (F) The densities of NCS-1 bands were expressed relative to the density of GAPDH bands in each tissue sample, and the group data is summarized (means ± SEM; $n = 3$).

Up-regulation of NCS-1 protein was also observed using a different type of stressor. Continuous treatment of neurons with colchicine for 4 d, which disrupts tubulin polymerization and blocks axonal transport, also increased NCS-1 expression levels (1.40 ± 0.03-fold above control levels; $P < 0.05$; $n = 4$), indicating that NCS-1 is up-regulated in vivo in response to two

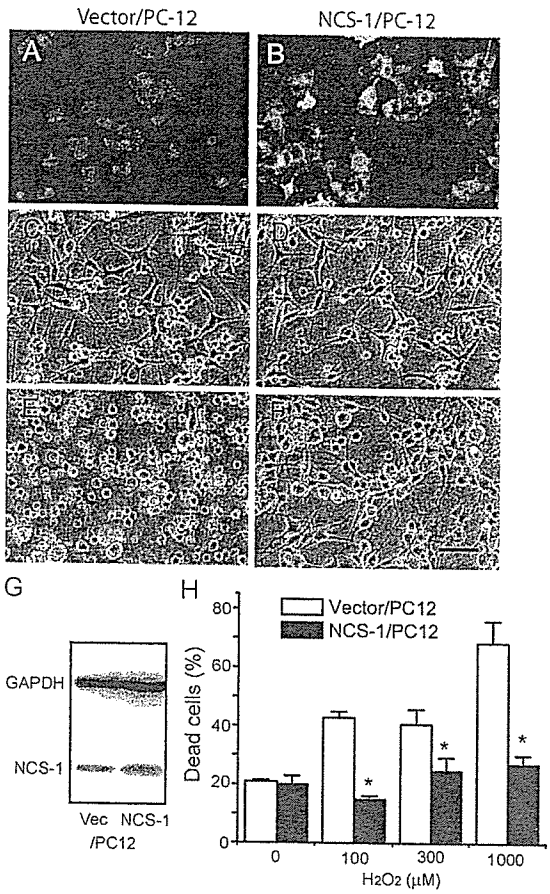

Figure 2. **Effects of the overexpression of NCS-1 on the susceptibility of PC-12 cells to H_2O_2 toxicity.** PC-12 cells stably transfected with NCS-1 (NCS-1/PC12) or vector alone (vector/PC-12) were differentiated into neuronlike cells by treatment with 100 ng/ml NGF and exposed to several concentrations (0–1 mM) of H_2O_2. (A and B) Immunofluorescent micrographs show that the expression level of NCS-1/PC12 cells is much higher than that in vector/PC12 cells. (C–F) Phase-contrast micrographs of PC-12 cells exposed to 0 (C and D) or 300 μM H_2O_2 for 3 d (E and F). Bar, 40 μm. (G) Representative immunoblots showing expression levels of NCS-1 in control vector and NCS-1–transfected cells. Also shown is the expression levels of the control protein GADPH obtained from immunoblots from the same cell samples. Unlike for NCS-1 levels, GADPH levels were not markedly different in control and NCS-1–transfected cells. (H) Bar graph shows the cell viability evaluated by trypan blue exclusion assay (means ± SEM [error bars]; $n = 8$). *, $P < 0.05$ versus vector/PC-12 cells.

different kinds of stressors—one being mechanical and the other being chemical injury.

Expression of NCS-1 renders PC-12 cells more tolerant to stressors

To study the physiological role of NCS-1 in damaged neurons, we next examined the effect of NCS-1 overexpression on the susceptibility of cells to several kinds of stressors. PC-12 cells stably transfected with either the NCS-1 expression vector (NCS-1/PC-12) or the vector alone (vector/PC-12) were differentiated into neuronlike cells, and the resistance to H_2O_2 toxicity was compared between these two groups. As shown in the immunofluorescent micrographs and immunoblot in Fig. 2 (A, B, and G), the expression level of NCS-1 was found to be significantly higher in NCS-1/PC-12 cells compared with vector-transfected cells, although these cells also had some endogenous NCS-1. Treatment with a relatively high dose (300 μM) of H_2O_2 for 3 d in the absence of pyruvate resulted in severe cellular damage in vector/PC-12 control cells; most cells were rounded up and detached from the substratum (Fig. 2 E). In contrast, the same treatment caused only a little damage to cells overexpressing NCS-1 (Fig. 2 F), indicating that the expression of NCS-1 rendered PC-12 cells more tolerant to H_2O_2 toxicity. The expression of NCS-1 reduced cell death caused by treatment with up to 1,000 μM H_2O_2 (Fig. 2 H). The aforementioned results were obtained from three cell lines transfected with NCS-1 and with corresponding vector-transfected control. A similar beneficial effect of NCS-1 on cell survival in response to 300 μM H_2O_2 was seen in two PC-12 cell lines that were not treated with NGF (not depicted).

NCS-1 promotes the long-term survival of primary cultured cortical neurons under stress and normal conditions

To further confirm the involvement of NCS-1 in neuronal survival, we overexpressed NCS-1 or its mutant E120Q in primary cultured embryonic rat cortical neurons that express endogenous NCS-1. The E120Q mutant possesses an amino acid substitution within the third EF-hand Ca^{2+}-binding motif, which impairs Ca^{2+} binding (Jeromin et al., 2004) but preserves the interaction with target proteins and, thereby, exerts a dominant-negative effect by disrupting the function of endogenous NCS-1 (Weiss et al., 2000). We used an adenoviral transfer system to transiently deliver the cDNA encoding NCS-1 together with EGFP (using an internal ribosome entry site–containing vector) and its E120Q mutant form into neurons cultured for 5 d in neurobasal medium containing B27 trophic supplements. As indicated by cells with EGFP fluorescence and nuclei stained with Hoechst 33258, nearly 70% of neurons were successfully infected with each virus at 3 d after infection (Fig. 3 A). We examined the effects of overexpression of wild-type and dominant-negative NCS-1 on neuronal survival under stress caused by B27 withdrawal, which has been reported to induce neuronal apoptosis (Brewer, 1995; Cheng et al., 2003). As shown in Fig. 3 B, B27 withdrawal promoted cell death in vector-treated control neurons (left; also compare the vector groups with and without B27 in Fig. 3 D). Overexpression of NCS-1, on the other hand, significantly rescued cells from death (Fig. 3 B, middle). In contrast, the expression of E120Q resulted in more severe cell death accompanying bleb formation (Fig. 3 B, right). To quantitatively analyze the time course for the changes in cell viability, the total number of surviving cells from the same field was counted daily by phase-contrast microscopy during 9 d (see Materials and methods). The results show that high cell viability was preserved upon expression of the wild-type NCS-1, whereas cell viability was reduced after the expression of E120Q; i.e., the number of days required to reach 70% cell viability were 5, 8, and 3 d for vector, NCS-1, and E120Q groups, respectively (Fig. 3 C). The expression levels of NCS-1 in each group of neurons before and after adenovirus infection in the absence of B27 trophic supplements are shown in the immunoblot (Fig. 3 E). Essentially the same results were obtained by counting neurons with condensed nuclei using

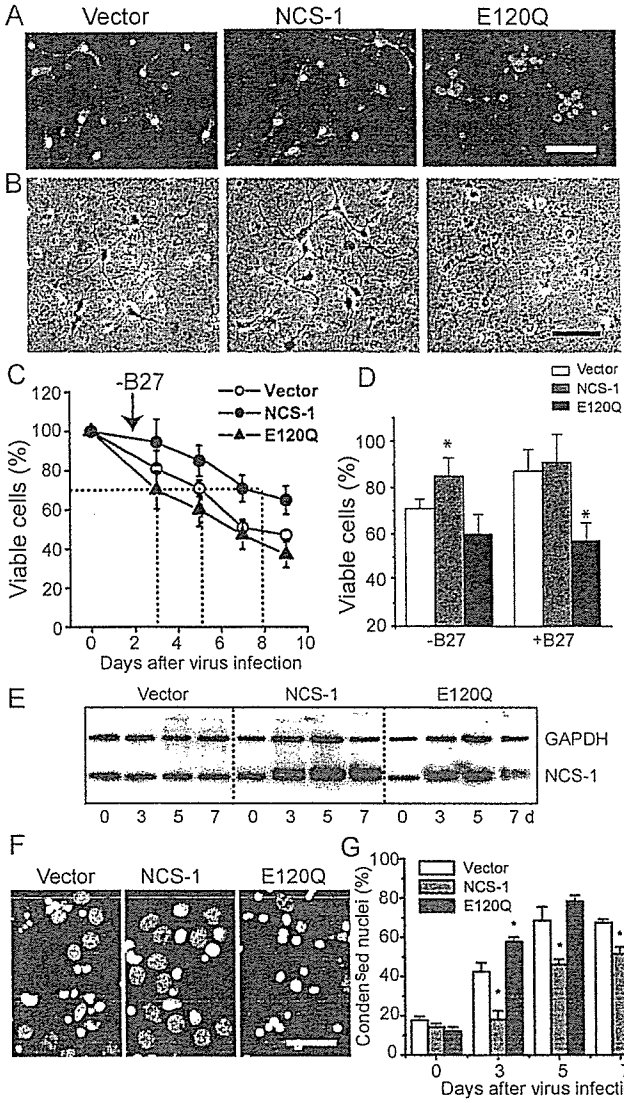

Figure 3. **Survival-promoting effect of NCS-1 in primary cultured cortical neurons.** Neurons were infected with adenovirus carrying EGFP vector alone, NCS-1, and its EF-hand mutant (E120Q) together with EGFP in the same internal ribosome entry site vector in culture medium containing neurobasal medium plus B27 trophic supplements, and they were further cultured in the presence or absence of B27 supplements (B27 supplements were withdrawn 2 d after the virus infections). (A) Fluorescent micrographs show the cultured neurons treated with adenovirus for 3 d (exhibiting strong EGFP signals) followed by treatment with a DNA-binding dye Hoechst 33258 to label their nuclei (red signals, pseudo-colored). (B) Phase-contrast micrographs show the cultured neurons treated with adenovirus for 5 d in the absence of B27 trophic supplements. Bars, 40 μm. (C) Time course of cell viability for neurons infected with adenovirus in the absence of B27 trophic supplements. Living neurons were counted daily by phase-contrast microscopy and plotted as a percentage of the initial number of neurons present on day 0 (n = 4). The number of days required to reach 70% cell viability is shown by the dotted lines. (D) Summary of cell viability data obtained from neurons cultured in the absence and presence of B27 trophic supplements at 5 d after virus infection. Error bars represent SEM. *, $P < 0.05$ versus the vector-controlled group. (E) Expression levels of NCS-1 and GAPDH in cultured neurons infected with each adenovirus indicated in the absence of B27 trophic supplements. (F and G) Staining patterns (light blue and white signals) of nuclei with Hoechst 33258 (F) and normalized numbers of cells having condensed nuclei (G). The dark blue color was changed to light blue or white to visualize signals more clearly. Bar, 15 μm.

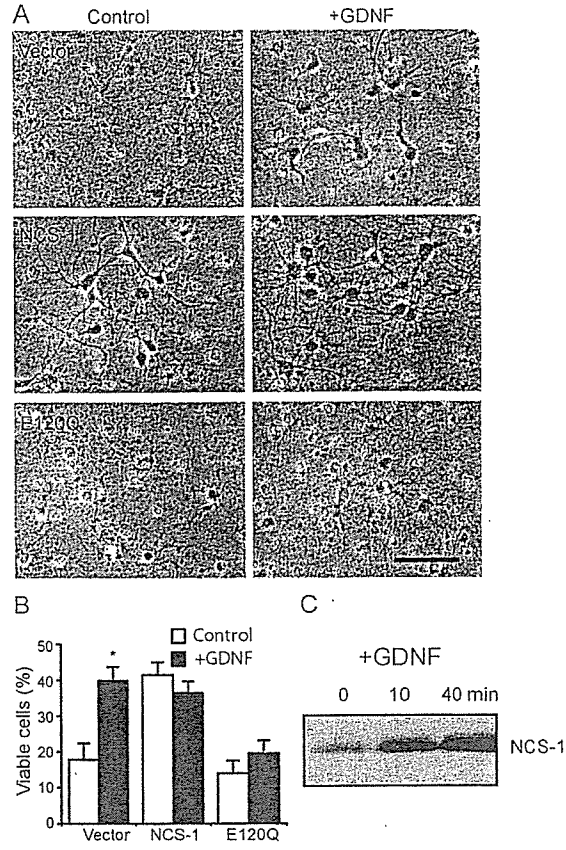

Figure 4. **NCS-1 mediates GDNF-induced neuronal survival.** (A) Primary cultured cortical neurons infected with adenovirus carrying vector alone (top), NCS-1 (middle), or E120Q mutant (bottom) were treated for 2 d with or without 10 ng/ml GDNF under the condition where B27 trophic supplement was depleted. Bar, 40 μm. (B) Summary of cell viability data. Viable cells were counted 2 d after GDNF treatment (+GDNF) or no treatment (control) and plotted as the percentage of the initial number of neurons present at day 0 in the same visual field (mean ± SEM [error bars]; n = 4). All neurons, not just transfected cells, were included in the cell viability counts. Note that treatment with E120Q largely prevented the GDNF-induced neuronal survival effect. *, $P < 0.05$ versus the data without exposure to GDNF. (C) Expression levels of NCS-1 in cultured neurons treated with 10 ng/ml GNDF for the indicated times.

Hoechst staining (Fig. 3, F and G), thus reinforcing the finding that the expression of NCS-1 protects neurons from cell death under apoptotic conditions. Furthermore, when B27 trophic supplement was kept in the culture medium (which is a less stress condition), the dominant-negative effect of E120Q was more clearly observed when compared with the vector control group (Fig. 3 D; also see A, where some blebs were observed in the neurons infected with E120Q mutant). In other preliminary experiments (not depicted), although the time course of the loss in cell viability was variable, overexpression of NCS-1 consistently delayed the loss of cell viability when B27 supplements were omitted, and the expression of E120Q always increased the rate of cell death when B27 was present. These results suggest that endogenous NCS-1 is playing an important role in keeping the long-term survival of cultured neurons under normal conditions in addition to the protective role from stress under apoptotic conditions.

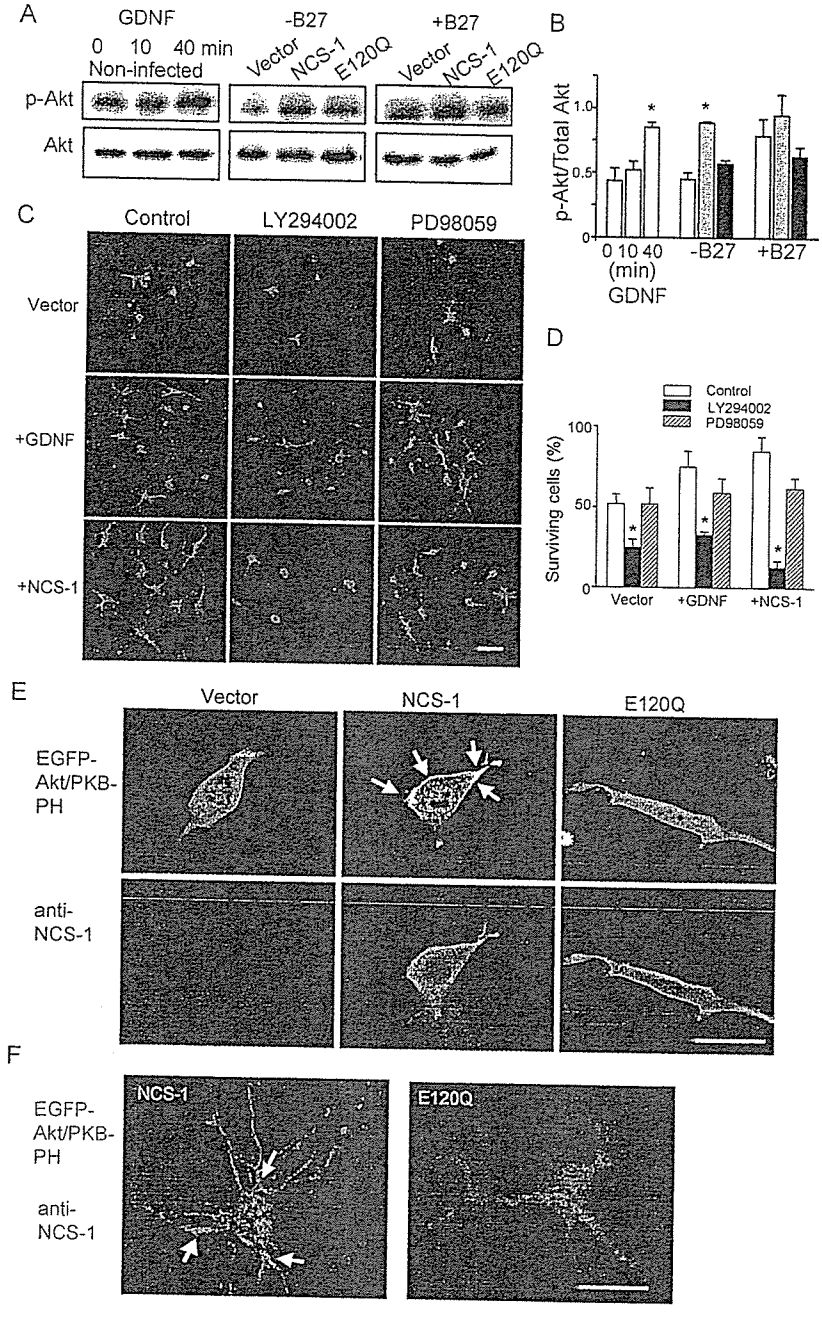

Figure 5. **NCS-1 promotes neuronal survival via activation of the PI3-K–Akt pathway.** (A and B) Both NCS-1 expression and GDNF treatment increase the phosphorylation of Akt kinase. Primary cultured cortical neurons were treated with 10 ng/ml GDNF for the indicated time periods or were infected with adenovirus carrying vector, NCS-1, or E120Q mutant and further incubated for 7 d in the presence or absence of B27 trophic supplements. They were then subjected to immunoblot analysis to detect protein levels of total (Akt) and phosphorylated form (p-Akt, the mixture of anti–P-Ser-473 and anti–P-Thr-308 antibodies, was used; A). The densities of phosphorylated Akt were normalized by those of total Akt levels and summarized in the bar graph (B). *, $P < 0.05$ versus vector control. (C and D) Both GDNF- and NCS-1–induced neuronal survival were abolished by PI3-K inhibitor but not by MEK inhibitor. Primary cultured cortical neurons were infected with adenovirus carrying NCS-1 or vector alone in medium lacking B27 trophic supplements. 3 d later, cultures were treated with 20 μM LY294002 or PD98059. For the vector-treated group, some cultures were further treated with 10 ng/ml GDNF. (C) Adenovirus-infected viable neurons treated or untreated with GDNF for 3 d. Bar, 40 μm. (D) Viable cells were counted and plotted as the percentage of the initial number of neurons present on day 0 (means ± SEM [error bars]; $n = 4$). *, $P < 0.05$ versus the data with no inhibitors. (E and F) NCS-1 activates Akt kinase by increasing the plasma membrane PtdIns(3,4)P_2 and PtdIns(3,4,5)P_3 levels in both CCL39 cells (E) and cultured neurons (F). CCL39 cells and primary cultured rat cortical neurons were transiently transfected with EGFP-Akt/PKB-PH together with either pCDNA3, NCS-1, or E120Q (1:3 ratios). 2 d later, cells were fixed, and immunocytochemistry was performed to detect NCS-1 proteins. Both EGFP distribution (E, top; and F, green signals) and NCS-1 expression (E, bottom; and F, red signals) were visualized using a laser confocal microscope. Laser confocal sections through the middle of representative cells in each treatment are shown. Arrows indicate the peripheral redistribution of the EGFP–PKB–PH in NCS-1–expressing cells. Bars, 10 μm.

NCS-1 mediates GDNF-induced cell survival

A large body of evidence suggests that neuronal survival is promoted by neurotrophic factors such as BDNF and GDNF (Boyd and Gordon, 2003). Because the long-term application of GDNF has been reported to enhance the expression of NCS-1 in *Xenopus laevis* motor neurons (Wang et al., 2001), we attempted to clarify the role of NCS-1 as a downstream mechanism of GDNF-induced cell survival in rat cortical neurons. When primary cultured cortical neurons were treated with 10 ng/ml GDNF for 2 d after the withdrawal of B27 supplements, neuronal survival was significantly enhanced when compared with time-matched control (Fig. 4, A [top] and B). Interestingly, the expression of NCS-1 mimicked the survival-promoting effects of GDNF; i.e., NCS-1 exerted a robust survival effect even in the absence of GDNF (Fig. 4, A [middle] and B). Most strikingly, the expression of the dominant-negative NCS-1 mutant E120Q largely prevented cell survival induced by GDNF (Fig. 4, A [bottom] and B). Immunoblot analysis revealed that the application of 10 ng/ml GDNF resulted in a significant increase in the expression level of endogenous NCS-1 within 10 min, which further increased at 40 min in these neurons (Fig. 4 C). The amount of NCS-1 remained elevated through 2 d of exposure to GDNF (not depicted). These results show that the treatment of GDNF increases the expression level of NCS-1, which subsequently promotes neuronal survival, suggesting that GDNF-induced neuroprotection is at least in part mediated by NCS-1.

Activation of the PI3-K-Akt pathway is involved in NCS-1-induced neuronal survival

In neurons, GDNF has been reported to promote cell survival via activation of signaling cascades involving the PI3-K–Akt pathway (Soler et al., 1999; Takahashi, 2001). In accordance with these studies, we also observed that exposure of primary cultured cortical neurons to GDNF resulted in a large increase in phospho-Akt levels (Fig. 5 A, left). Therefore, it was of interest for us to test whether NCS-1 also activates this kinase. We examined the effect of NCS-1 expression or its dominant-negative form on Akt phosphorylation in the presence or absence of B27 trophic supplements. When B27 trophic supplements were absent, the expression of NCS-1 significantly enhanced the phosphorylation of Akt, whereas expression of the dominant-negative mutant E120Q had little effect when compared with control vector-infected neurons (Fig. 5, A [middle] and B). On the other hand, when B27 supplements were present, a relatively high level of phosphorylated Akt was observed in the vector-treated control group (Fig. 5, A [right] and B). Additional expression of exogenous NCS-1 further increased the Akt phosphorylation level, whereas expression of the dominant-negative mutant suppressed phosphorylation (Fig. 5, A [right] and B). Thus, the phosphorylation levels of Akt in each group of neurons were well correlated with their viabilities, as shown in Fig. 3 D.

In addition, pretreatment of cultured cortical neurons with LY294002, an inhibitor of PI3-K, completely abolished both GDNF- and NCS-1–induced neuronal survival, whereas PD98059, an inhibitor of MAPK kinase (MEK), did not (Fig. 5, C and D). These results suggest that the NCS-1–induced survival-promoting effect is mediated via the PI3-K–Akt pathway but not the MAPK pathway in cultured cortical neurons.

To further understand the upstream mechanism of the NCS-1–induced activation of Akt, we next examined the effect of overexpression of NCS-1 and E120Q on the subcellular localization of Akt/PKB in living cells. Akt/PKB is known to be translocated to the plasma membrane when it is fully activated upon phosphorylation and bound with its substrates PtdIns(3,4)P_2 and PtdIns(3,4,5)P_3 (Alessi et al., 1996). We constructed the GFP-tagged pleckstrin homology (PH) domain of Akt/PKBα (EGFP-Akt/PKB-PH) and transiently cotransfected it into CCL39 cells, which express a small amount of endogenous NCS-1, together with NCS-1, E120Q, or empty vector. 2 d later, the subcellular localization of EGFP-tagged Akt/PKB-PH was assessed on a confocal microscope. Akt/PKB-PH was diffusely localized in the cytosol of vector-transfected control cells (Fig. 5 E). Interestingly, Akt/PKB-PH became localized in the peripheral region of cells when NCS-1 was coexpressed, but this peripheral localization was abolished when E120Q was coexpressed (Fig. 5 E). Qualitatively similar results were also obtained when primary cultured cortical neurons were treated with the same vectors; i.e., Akt/PKB-PH was localized in the peripheral regions of neurons when NCS-1 was overexpressed, but a more diffuse localization pattern was observed when E120Q was overexpressed (Fig. 5 F). The distribution pattern of Akt/PKB-PH in vector-transfected neurons was similar to that of NCS-1–overexpressing cells (not depicted). These results strongly demonstrate that NCS-1 increases the levels of plasma membrane PtdIns(3,4)P_2 and PtdIns(3,4,5)P_3 and, thus, activates Akt/PKB in living cells.

Dominant-negative NCS-1 accelerates the in vivo axotomy-induced loss of neurons

We examined the effects of the overexpression of NCS-1 and its dominant-negative mutant on the survival of these neurons to clarify the physiological role of NCS-1 in injured motor neurons in vivo. One side of vagus nerves of adult rats were axotomized as previously described (Fig. 1) and infected with adenoviral vectors encoding NCS-1, E120Q, or EGFP vector alone, and neuronal degeneration was evaluated by histological analysis. 1 wk after axotomy, nearly 30% of nerve cells were found to be EGFP positive in the injured side (Fig. 6 A). There were clear differences in the staining pattern between control and injured sides for all groups, probably because the regeneration process, such as activation of the surrounding glial cells, was ongoing on injured sides. However, the number of surviving motor neurons stained with hematoxylin were not significantly decreased at the injured side for vector-treated DMV sections (Fig. 6, B and D; examples of counted neurons are indicated by black arrows in C). This would probably be the result of natural antiapoptotic mechanisms induced by injury, which exist in mature neurons as previously reported (Benn and Woolf, 2004). Because the expression level of NCS-1 was significantly increased in response to in vivo axotomy (Fig. 1), we hypothesized that NCS-1 may be involved in this antiapoptotic mechanism. If so, blocking of endogenous NCS-1 would reduce this beneficial effect. As expected, the dominant-negative E120Q mutant resulted in a significant loss of neurons in the injured side (Fig. 6, B–D), and some TUNEL-positive nuclei were also detected only in this group (Fig. 6 E, arrows; and its magnified image in F). Considering that the infection efficiency was only ~30% in these experiments, a large majority of neurons successfully infected with E120Q appear to have undergone apoptosis. Infection of neurons with the functional NCS-1 adenovirus only had a modest effect on neuronal survival. This probably results from both the low infection efficiency and the high levels of endogenous NCS-1 expression in axotomized neurons (Fig. 1) because the NCS-1 effects are already close to maximum. Thus, the dominant-negative mutant E120Q inhibited the survival of adult DMV neurons from axotomy-induced injury, strongly suggesting that NCS-1 is one of the important factors mediating neuronal survival after in vivo axotomy.

Discussion

Numerous stressors, including physical or chemical injury and genetic abnormalities, lead to neuronal degeneration by programmed cell death along an apoptotic pathway. Under these conditions, some intrinsic and extrinsic factors, including neurotrophic factors, are known to activate the antiapoptotic process to rescue neurons from death. However, the signaling pathway leading to cell survival is not yet completely understood.

In this study, we identified a novel function for the Ca^{2+}-binding protein NCS-1, which (1) promotes the long-term survival

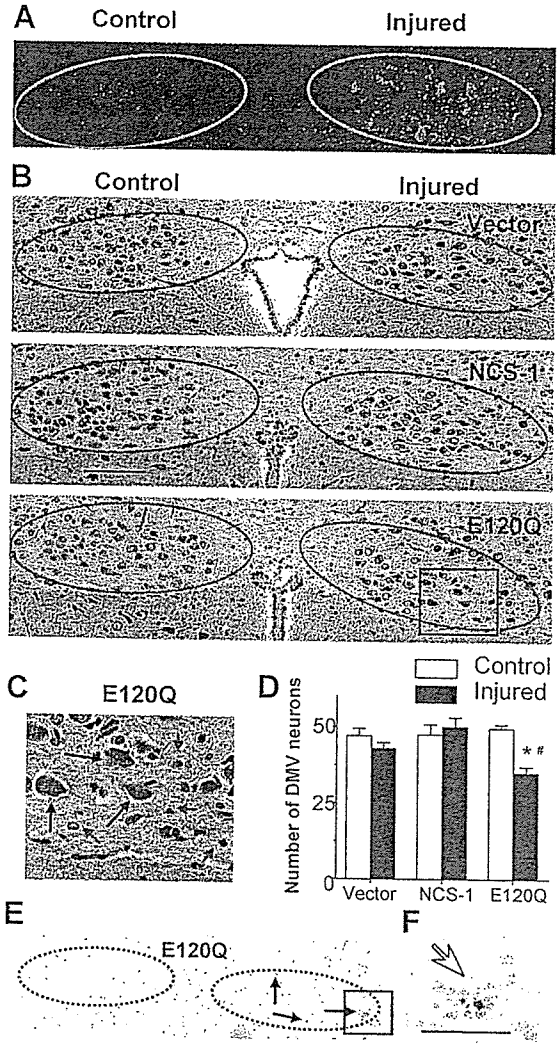

Figure 6. **Dominant-negative NCS-1 mutant E120Q promotes the axotomy-induced degeneration of DMV neurons.** After the axotomy of vagus motor neurons were performed as described in Fig. 1, adenoviral vectors carrying NCS-1, E120Q, or EGFP alone were injected from the stump of the nerve. 1 wk after the treatment, the brainstem was excised, and serial sections were cut. (A) Representative EGFP fluorescence image showing that EGFP signals were detected in some cells on the injured side. Positions of DMV neurons are indicated by circles in A, B, and E. (B) Histological evaluation of DMV neurons in adenovirus-treated animals by hematoxylin/eosin staining. (C) Magnified image of the boxed area in B for E120Q-treated DMV neurons. Only neurons (indicated by black arrows), not nuclei, of glial or endothelial cells (indicated by red arrows) were counted. (D) Summarized data obtained from B. *, $P < 0.05$ versus the control side of the same section. #, $P < 0.05$ versus the injured side of vector-treated animals (means ± SEM [error bars]; $n = 6$ from three animals). (E) An example of the TUNEL-staining pattern obtained from an E120Q-treated animal. (F) The magnified image of the boxed area in E. TUNEL-positive nuclei are indicated by arrows. Bar (B), 100 μm; (F) 25 μm.

of cultured neurons via PI3-K–Akt signaling pathways; (2) mediates, at least in part, GDNF-induced neuroprotection; and (3) is up-regulated in response to axonal injury and plays an important role in the antiapoptotic mechanism in injured motor neurons.

NCS-1 is a novel survival-promoting factor in neuronal cells

We observed that the overexpression of NCS-1 rendered PC-12 cells and primary cultured cortical neurons more tolerant to several kinds of stressors, such as oxidative stress or trophic supplement withdrawal (Figs. 2 and 3), demonstrating that the expression of NCS-1 protects neurons from cell death under apoptotic conditions. In addition, overexpression of an EF-hand dominant-negative mutant E120Q significantly accelerated apoptosis when B27 trophic supplements were kept in the culture medium (Fig. 3 D), suggesting that endogenous NCS-1 is important for keeping the long-term survival of cultured neurons under normal (or less apoptotic) conditions. The latter finding also indicates that Ca^{2+} binding is required for NCS-1–mediated cell survival. On the basis of these findings, we propose that NCS-1 is a novel member of survival-promoting factors in cultured neurons.

NCS-1 mediates GDNF-induced cell survival via activation of the PI3-K-Akt survival pathway

We found that treatment of cultured cortical neurons with a neurotrophic factor GDNF increased the expression level of NCS-1 (Fig. 4 C) and enhanced neuronal survival (Fig. 4, A and B), which is consistent with a previous study reporting that GDNF enhanced the expression of frequenin/NCS-1 in *Xenopus* motor neurons (Wang et al., 2001). GDNF-induced increase in the NCS-1 level appeared to be caused by the synthesis of protein and/or mRNA but not by the prevention of NCS-1 degradation because GDNF did not raise the expression level of NCS-1 in the presence of the inhibitor of protein synthesis cycloheximide (10 μg/ml for 20 h; not depicted). In contrast to the vector-treated control neurons, GDNF did not further enhance the survival effect in neurons overexpressing NCS-1 (Fig. 4, A and B), suggesting that cell viability was already sufficiently high under this condition. Strikingly, the survival-promoting effect of GDNF was largely prevented by overexpression of the dominant-negative mutant E120Q (Fig. 4, A and B), suggesting that NCS-1 mediates the GDNF survival signal.

GDNF activates at least two intracellular pathways in neurons: one involving the PI3-K–Akt pathway and another involving the MAPK (p42 and p44, also called ERK1 and ERK2) pathway. However, PI3-K but not the MAPK pathway has been reported to be responsible for GDNF-mediated neuronal survival in motor neurons (Soler et al., 1999). In accordance with this study, we observed that exposure of primary cultured cortical neurons to GDNF resulted in a large increase in the phospho-Akt level (Fig. 5 A). In the same way, the overexpression of NCS-1 also dramatically enhanced the phosphorylation levels of Akt both in the presence and absence of B27 trophic supplements, whereas the overexpression of dominant-negative mutant E120Q did not (Fig. 5 A). In addition, the NCS-1–nduced survival-promoting effect was largely inhibited by the PI3-K inhibitor LY294002 but not the MEK inhibitor PD98059 (Fig. 5, C and D). Furthermore, NCS-1 increased the plasma membrane PtdIns(3,4)P_2 and PtdIns(3,4,5)P_3 levels, which indicates the activation of Akt in intact cells (Fig. 5, E and F). These results strongly suggest that NCS-1 is a novel downstream target that mediates GDNF survival signal through activation of the PI3-K–Akt pathway.

Possible mechanisms of the action of NCS-1

Several possible mechanisms may underlie the survival action of NCS-1. We observed that Akt/PKB-PH was recruited to the plasma membrane when NCS-1 was coexpressed, suggesting that NCS-1 acts upstream of the Akt pathway. NCS-1 was previously reported to activate PI4-K (Hendricks et al., 1999), which increases the level of plasma membrane PtdIns(4)P, the substrate of PI3-K, as well as PI5-K. Therefore, upon activation of these kinases, other phosphoinositides would be produced. Indeed, it has been reported that the overexpression of NCS-1 significantly increased both PtdIns(4)P and PtdIns(4,5)P_2 levels in PC-12 cells (Koizumi et al., 2002). Furthermore, PtdIns(3,4)P_2 and PtdIns(3,4,5)P_3, the substrates of Akt/PKB, would also be produced, which, in turn, would activate the Akt pathway (Cantley, 2002). As expected, the overexpression of NCS-1 increased the plasma membrane PtdIns(3,4)P_2 and PtdIns(3,4,5)P_3 levels both in CCL39 cells and neuronal cells (Fig. 5, E and F), enhanced the phosphorylation of Akt (Fig. 5 A), and promoted neuronal survival (Fig. 3). Therefore, we propose that activation of such a phosphatidylinositol pathway is a mechanism for the survival action of NCS-1. In addition, we observed that in contrast to GDNF, our preliminary data show that BDNF did not increase the expression level of NCS-1 (unpublished data) despite the reported survival-promoting effect of BDNF in cultured cortical neurons (Cheng et al., 2003). Interestingly, BDNF-induced survival signaling has been reported to be mediated by CaM, another Ca^{2+}-binding protein in cortical neurons (Cheng et al., 2003), and CaM has been reported to directly activate PI3-K (Perez-Garcia et al., 2004). Therefore, NCS-1 mediates the GDNF signal by activating PI4-K, whereas CaM mediates the BDNF signal by activating PI3-K. These two signals would lead the survival signal to the Akt pathway.

On the other hand, it is also possible that NCS-1 promotes neuronal survival by some other mechanisms in addition to activation of the Akt pathway. For example, the survival-promoting effect of NCS-1 appears to be analogous to that of the recently characterized antiapoptotic protein family called inhibitors of apoptosis, which suppress apoptosis through the direct inhibition of caspases (Liston et al., 2003). Some of these proteins, such as neuronal apoptosis inhibitory protein and X-linked inhibitors of apoptosis protein, have been reported to be essential for GDNF-mediated neuroprotective effects in injured motor neurons in vivo (Perrelet et al., 2002). Furthermore, recent evidence demonstrates that neuronal apoptosis inhibitory protein interacts with hippocalcin, another closely related Ca^{2+}-binding protein that affects caspase-12 activity (Korhonen et al., 2005) and protects neurons against Ca^{2+}-induced cell death (Mercer et al., 2000). Therefore, we do not exclude the possibility that like these proteins, NCS-1 also exerts a more direct effect on some caspases. We are currently investigating the possible interaction of these proteins.

As NCS-1 is known to interact with voltage-gated K^+ channels (Kv4; Nakamura et al., 2001), it might also increase the resistance of neurons to excitotoxic apoptosis through the activation of K^+ channels. Increased outward K^+ current would prevent neurons from reaching firing threshold and, thereby, prevent cells from Ca^{2+} overload leading to cell death.

NCS-1 is a novel survival-promoting factor up-regulated in injured neurons

In this study, we found that the expression level of NCS-1 was significantly increased in response to axonal injuries (transection of the vagus nerve as well as treatment of nerves with colchicine) in the DMV neurons of adult rats (Fig. 1). The behavior of NCS-1 appears to be analogous to that of the recently identified protein damage-induced neuronal endopeptidase, which is expressed in response to neuronal damages induced by nerve transection and colchicine treatment in both the central and peripheral nervous systems (Kiryu-Seo et al., 2000). Because antiapoptotic mechanisms are activated in mature neurons in response to stress to protect against accidental apoptotic cell death, it has been described that peripheral axotomy in adult neurons does not result in extensive cell death (Benn and Woolf, 2004). In accordance with this, we also observed that little loss of motor neurons was evident by in vivo axotomy in vector-treated control neurons (Fig. 6, B and D). The expression of exogenous NCS-1 did not exert the further beneficial effect (Fig. 6, B and D). This marginal effect of exogenous NCS-1 (compared with the vector control group) would be the result of the increased expression level of endogenous NCS-1 in axotomized neurons, which occurs for all groups. In contrast, overexpression of dominant-negative E120Q significantly decreased the number of surviving neurons (Fig. 6, B–D) and produced TUNEL-positive apoptotic neurons at the injured side (Fig. 6, E and F), indicating that disruption of NCS-1 function increased the vulnerability of DMV neurons to axotomy.

Overexpression of NCS-1 rendered PC-12 cells resistant to H_2O_2 toxicity even in the absence of GDNF (Fig. 2), suggesting that NCS-1 itself is enough to promote cell survival. This is consistent with our view that NCS-1 is the downstream target for GDNF. Because growing evidence indicates that nerve injury leads to the up-regulation of multiple antiapoptotic molecules, including GDNF (Liberatore et al., 1997; Yamamoto et al., 1998; Wang et al., 2002), it is possible that neuronal damages induced by in vivo axotomy enhance the synthesis and/or secretion of GDNF, which, in turn, up-regulates NCS-1 expression and promotes neuronal survival in injured neurons. Although an underlying mechanism would be different, the up-regulation of NCS-1 has also been reported in the cortex of schizophrenic and bipolar patients, demonstrating the involvement of NCS-1 in neurological disease (Koh et al., 2003).

In conclusion, we characterized a novel function of NCS-1 mediating a GDNF-induced neuroprotective effect via activations of Akt kinase. Furthermore, we found that NCS-1 is up-regulated in response to nerve injury and plays an important role in the antiapoptotic mechanism in adult motor neurons. Our present findings would provide new and basic insights into the mechanism of neuronal regeneration.

Materials and methods

Plasmids and viral vectors

E120Q NCS-1 point mutant was generated with a conventional PCR protocol using the wild-type rat NCS-1 (GenBank/EMBL/DDBJ accession no. L27421 as a template and was sequenced to confirm the mutation.

Akt/PKBα cDNA was cloned from the human kidney cDNA library (CLONTECH Laboratories, Inc.), and NH_2-terminally tagged fluorescent protein EGFP-Akt/PKB-PH was constructed incorporating a fragment of 750 bp, encoding the first 250 amino acids of PKBα (containing the PH domain) into EGFP-vector as described previously (Currie et al., 1999).

Adenovirus containing wild-type NCS-1 and the E120Q mutant inserts were generated by cotransfecting either of these plasmids and pBHG11 (Microbix Biosystems, Inc.) into HEK 293 cells. Viral DNA was isolated from the supernatant in the wells displaying the cytopathic effect. Replication-incompetent virus containing DNA inserts were plaque-purified twice and grown on HEK 293 cells to produce large amounts of adenovirus. Tissue culture supernatant containing adenovirus was concentrated by centrifugation over cesium chloride. The titers of viral stocks were 2.2×10^{10} pfu/ml for EGFP–NCS-1, 1.1×10^{10} pfu/ml for EGFP-E120Q, and 2.2×10^{10} pfu/ml for EGFP-vector.

Cell cultures

PC-12 cells stably transfected with vector alone or vector containing cDNA coding for the wild-type NCS-1 (several clones) were grown onto collagen-coated (500 μg/ml of type I; Sigma-Aldrich) culture dishes in growth medium (DME containing 10% horse serum, 5% FBS, and 400 μg/ml geneticin and gentamicin) as described previously (Koizumi et al., 2002). When cells became 80% confluent, they were switched to the differentiation medium (growth medium with half serum) supplemented with 100 ng/ml NGF-7S (Invitrogen).

Primary culture of cortical neurons was performed using the cortex from Sprague-Dawley rats at embryonic day 18. In brief, cortical tissues were isolated from whole brain, minced into small pieces, and digested for 10 min at 37°C in a 20-U/ml papain solution containing 0.002% DNase I (Worthington Biochemical Corp.). After titration of the enzymatic activity, cells were mechanically dissociated by several passages through pipette tips. After centrifugation, cells were resuspended in neurobasal medium supplemented with B27 trophic factors (both from Invitrogen), whose compositions were reported previously (Brewer et al., 1993). They were then plated onto culture dishes coated with 0.1% polyethylenimine at a density of $2.5–5 \times 10^4$ cells/cm^2 for cell survival assay and 10^5 cells/cm^2 for immunoblot analysis.

Fluorescent microscopy

CCL39 cells and primary cultured rat cortical neurons were plated onto collagen-coated glass coverslips and cultivated for 1 d. They were then transiently transfected with the EGFP-Akt/PKB-PH construct together with either NCS-1, E120Q, or pCDNA3 (1:3 ratio) using LipofectAMINE 2000 (Invitrogen) and were subjected to immunocytochemistry. In brief, cells were fixed with 4% PFA, permeabilized with 0.2% Triton X-100, and blocked with 5% BSA. They were then incubated for 1 h with anti–NCS-1 antibody (1:200) followed by incubation with secondary antibodies (FITC- or rhodamine-conjugated goat anti–rabbit IgG; 1:200; Jackson ImmunoResearch Laboratories). After extensive wash with PBS, cell images were scanned on a laser confocal microscope (MRC-1024K; Bio-Rad Laboratories) or obtained with conventional epifluorescence illumination (BX50WI; Olympus) with a cooled CCD camera (CoolSNAP; Photometrics) using a 0.9-W 60× water immersion objective lens. Immunocytochemistry for PC-12 cells were also performed in the same way.

Evaluation of neuronal survival

The primary cultured neurons were infected with viruses at a multiplicity of infection of 100 pfu/cell at 5 d after plating. Under this condition, we found that nearly 70% of the neurons were infected by monitoring EGFP fluorescence (Fig. 3 A). The number of living neurons was counted within the fixed area of images taken by a digital camera (Coolpix 4500; Nikon). To count the number of cells always within the same area, a grid seal with numbering (Asahi Techno glass) was stuck on the bottom of each culture dish. The number of living neurons remaining at each day was expressed as a percentage of the initial number. Neurons showing the degenerating stage characterized by nuclear condensation, membrane blebbing, or extensive neurite fragmentation were excluded. Four different regions were selected from one dish, and six separate experiments were performed for each condition.

To identify and quantify apoptotic neurons, cells were fixed with 4% PFA and were stained with Hoechst 33258. Coverslips were mounted onto glass slides, and cells were observed under epifluorescence illumination on an inverted microscope (1X71; Olympus) using a 40× NA 1.35 oil immersion objective lens (Olympus). Cells were considered apoptotic if their nuclear chromatin was condensed or fragmented, whereas cells were considered viable if their chromatin was diffusely and evenly distributed throughout the nucleus (Fig. 3 F).

Immunoblot analysis

DMV tissue samples were obtained by scratching the DMV neurons from several frozen sections of brainstem (described in the next section) using pulled glass capillary under the light microscope. These tissue samples or cultured cells (PC-12 cells and cortical neurons) were then solubilized in SDS-PAGE sample buffer containing protease and phosphatase inhibitors and subjected to immunoblot analysis using image density software (Scion Image; Scion Corp.) as previously described (Nakamura et al., 2001). Primary antibodies used were anti–NCS-1 antibody (1:1,000), which was previously described (Jeromin et al., 1999), and publicly available antibodies: monoclonal anti-GAPDH antibody (1:1,000) obtained from Chemicon as well as antiphospho-Akt antibody (detectable for the phosphorylation of Thr308 and Ser473; 1:1,000) and anti-Akt antibody (1:1,000; both from Cell Signaling Technology). Secondary antibodies used were HRP-conjugated anti–rabbit and anti–mouse antibodies or a combination of biotinylated anti–rabbit (or mouse) antibodies (Zymed Laboratories) and HRP-conjugated streptavidin (Zymed Laboratories).

In vivo axotomy and colchicine treatment

The method of vagus axotomy was described previously (Nabekura et al., 2002a). In brief, 4–6-wk-old Sprague-Dawley rats were deeply anesthetized with 50 mg/kg pentobarbital, and axotomy of the vagus motor neurons was performed with fine scissors at the unilateral vagus nerve at the neck. Injured neurons were confirmed by detecting the fluorescence of Di-I in the DMV, which had been placed at the proximal cut site of the nerve bundle (Nabekura et al., 2002a).

To test the effects of colchicine, an implantable polymer containing 10% (wt/vol) colchicine was made by mixing colchicine with ethylene-vinyl acetate copolymer (Elvax) followed by drying as described previously (Kakizawa et al., 2000). Solid slices (~1 mm^2) were placed around the unilateral vagal nerve to allow the continuous release of colchicine from slices. The skin incision was closed, and rats were returned to the cage after awaking from the anesthetic.

Histology

1 d to 2 mo (usually 1 wk) after receiving ipsilateral vagal axotomy, brainstems were quickly removed, and 8–10-μm-thick frozen sections were cut. Immunohistochemistry was performed using the labeled biotin–streptavidin method. In brief, after fixation and blocking, the sections were incubated at 4°C overnight with a rabbit polyclonal antibody against NCS-1 at a dilution of 1:15,000 and were sequentially incubated with a biotinylated anti–rabbit secondary antibody and a HRP-conjugated streptavidin–biotin complex (GE Healthcare). The colored reaction product was developed with DAB solution. The sections were lightly counterstained with hematoxylin to visualize nuclei. Images were acquired using a digital camera (FX380; Olympus) equipped with an image filing software (FLVFS-LS; Flovel).

Comparison of the expression level of NCS-1 between injured and control sides were performed using computerized image analysis (Win Roof; Mitani Corp.). In brief, the DMV region from the injured side was at first selected, and the image was converted to binary images by thresholding so that only the area highly stained with anti–NCS-1 antibody could be detected. The same threshold level was used for both the control and injured DMV in each tissue section. The highly stained area was summated and represented as normalized values.

Neuronal degeneration was evaluated by counting surviving neurons as described previously (Rothstein et al., 2005) as well as by TUNEL staining using the apoptag peroxidase in situ Apoptosis Detection Kit (Chemicon). In brief, in vivo axotomy was performed as described above, and, at the same time, adenoviral vectors carrying EGFP only, EGFP plus NCS-1, or E120Q (10^9 pfu each) was injected into the stump of the nerve using a 34-gauge needle. 1 wk after axotomy, paraffin-embedded serial sections (3–4 μm) were made from the brainstem. After they were deparaffinized, sections were directly stained with hematoxylin/eosin to visualize the structure of the DMV region. TUNEL staining was performed in accordance with the manufacturer's method. The sections were lightly counterstained with methyl green. Control sections were treated similarly but incubated in the absence of TdT enzyme. To confirm whether the adenoviral vectors were transferred to the DMV neurons, another set of animals were treated in the same way. 8-μm frozen sections were cut 1 wk after operation, and EGFP signals were viewed under a fluorescence microscope (1X71; Olympus). All image acquisitions were performed at room temperature, and images were subsequently processed using Adobe Photoshop (version 7) and Adobe Illustrator (version 10) software. All experiments conformed to the Guiding Principles for the Care and Use of Animals approved by the Council of the Physiological Society of Japan. All efforts were made to minimize the number of animals used and their suffering.

Statistics

Comparisons between two groups were performed using the paired or unpaired *t* test. Values of $P < 0.05$ were considered statistically significant. All summarized data are expressed as means ± SEM.

We thank Dr. Andrew Moorhouse (The University of New South Wales, Sydney, Australia) for critical reading of this manuscript. We also thank Dr. Takeharu Nishimoto and Dr. Hideo Nishitani (Kyushu University, Fukuoka, Japan) for useful discussions of this study.

This work was supported, in part, by a Grant-in-Aid for Scientific Research (17590196) and Priority Areas (13142210) from the Ministry of Education, Culture, Sports, Science and Technology of Japan and the Japan Heart Foundation and by a grant from the National Institutes of Health/National Institute of Neurological Disorder and Stroke (NS38126).

Submitted: 24 August 2005
Accepted: 17 February 2006

References

Alessi, D.R., M. Andjelkovic, B. Caudwell, P. Cron, N. Morrice, P. Cohen, and B.A. Hemmings. 1996. Mechanism of activation of protein kinase B by insulin and IGF-1. *EMBO J.* 15:6541–6551.

Benn, S.C., and C.J. Woolf. 2004. Adult neuron survival strategies–slamming on the brakes. *Nat. Rev. Neurosci.* 5:686–700.

Boyd, J.G., and T. Gordon. 2003. Neurotrophic factors and their receptors in axonal regeneration and functional recovery after peripheral nerve injury. *Mol. Neurobiol.* 27:277–324.

Brewer, G.J. 1995. Serum-free B27/neurobasal medium supports differentiated growth of neurons from the striatum, substantia nigra, septum, cerebral cortex, cerebellum, and dentate gyrus. *J. Neurosci. Res.* 42:674–683.

Brewer, G.J., J.R. Torricelli, E.K. Evege, and P.J. Price. 1993. Optimized survival of hippocampal neurons in B27-supplemented Neurobasal, a new serum-free medium combination. *J. Neurosci. Res.* 35:567–576.

Cantley, L.C. 2002. The phosphoinositide 3-kinase pathway. *Science.* 296:1655–1657.

Chen, X.L., Z.G. Zhong, S. Yokoyama, C. Bark, B. Meister, P.O. Berggren, J. Roder, H. Higashida, and A. Jeromin. 2001. Overexpression of rat neuronal calcium sensor-1 in rodent NG108-15 cells enhances synapse formation and transmission. *J. Physiol.* 532:649–659.

Cheng, A., S. Wang, D. Yang, R. Xiao, and M.P. Mattson. 2003. Calmodulin mediates brain-derived neurotrophic factor cell survival signaling upstream of Akt kinase in embryonic neocortical neurons. *J. Biol. Chem.* 278:7591–7599.

Currie, R.A., K.S. Walker, A. Gray, M. Deak, A. Casamayor, C.P. Downes, P. Cohen, D.R. Alessi, and J. Lucocq. 1999. Role of phosphatidylinositol 3,4,5-trisphosphate in regulating the activity and localization of 3-phosphoinositide-dependent protein kinase-1. *Biochem. J.* 337:575–583.

Gomez, M., E. De Castro, E. Guarin, H. Sasakura, A. Kuhara, I. Mori, T. Bartfai, C.I. Bargmann, and P. Nef. 2001. Ca^{2+} signaling via the neuronal calcium sensor-1 regulates associative learning and memory in *C. elegans*. *Neuron.* 30:241–248.

Henderson, C.E., H.S. Phillips, R.A. Pollock, A.M. Davies, C. Lemeulle, M. Armanini, L. Simmons, B. Moffet, R.A. Vandlen, L.C. Simpson, et al. 1994. GDNF: a potent survival factor for motoneurons present in peripheral nerve and muscle. *Science.* 266:1062–1064.

Hendricks, K.B., B.Q. Wang, E.A. Schnieders, and J. Thorner. 1999. Yeast homologue of neuronal frequenin is a regulator of phosphatidylinositol-4-OH kinase. *Nat. Cell Biol.* 1:234–241.

Jeromin, A., A.J. Shayan, M. Msghina, J. Roder, and H.L. Atwood. 1999. Crustacean frequenins: molecular cloning and differential localization at neuromuscular junctions. *J. Neurobiol.* 41:165–175.

Jeromin, A., D. Muralidhar, M.N. Parameswaran, J. Roder, T. Fairwell, S. Scarlata, L. Dowal, S.M. Mustafi, K.V. Chary, and Y. Sharma. 2004. N-terminal myristoylation regulates calcium-induced conformational changes in neuronal calcium sensor-1. *J. Biol. Chem.* 279:27158–27167.

Kakizawa, S., M. Yamasaki, M. Watanabe, and M. Kano. 2000. Critical period for activity-dependent synapse elimination in developing cerebellum. *J. Neurosci.* 20:4954–4961.

Kirik, D., B. Georgievska, and A. Bjorklund. 2004. Localized striatal delivery of GDNF as a treatment for Parkinson disease. *Nat. Neurosci.* 7:105–110.

Kiryu-Seo, S., M. Sasaki, H. Yokohama, S. Nakagomi, T. Hirayama, S. Aoki, K. Wada, and H. Kiyama. 2000. Damage-induced neuronal endopeptidase (DINE) is a unique metallopeptidase expressed in response to neuronal damage and activates superoxide scavengers. *Proc. Natl. Acad. Sci. USA.* 97:4345–4350.

Koh, P.O., A.S. Undie, N. Kabbani, R. Levenson, P.S. Goldman-Rakic, and M.S. Lidow. 2003. Up-regulation of neuronal calcium sensor-1 (NCS-1) in the prefrontal cortex of schizophrenic and bipolar patients. *Proc. Natl. Acad. Sci. USA.* 100:313–317.

Koizumi, S., P. Rosa, G.B. Willars, R.A. Challiss, E. Taverna, M. Francolini, M.D. Bootman, P. Lipp, K. Inoue, J. Roder, and A. Jeromin. 2002. Mechanisms underlying the neuronal calcium sensor-1-evoked enhancement of exocytosis in PC12 cells. *J. Biol. Chem.* 277:30315–30324.

Korhonen, L., I. Hansson, J.P. Kukkonen, K. Brannvall, M. Kobayashi, K. Takamatsu, and D. Lindholm. 2005. Hippocalcin protects against caspase-12-induced and age-dependent neuronal degeneration. *Mol. Cell. Neurosci.* 28:85–95.

Liberatore, G.T., J.Y. Wong, M.J. Porritt, G.A. Donnan, and D.W. Howells. 1997. Expression of glial cell line-derived neurotrophic factor (GDNF) mRNA following mechanical injury to mouse striatum. *Neuroreport.* 8:3097–3101.

Liston, P., W.G. Fong, and R.G. Korneluk. 2003. The inhibitors of apoptosis: there is more to life than Bcl2. *Oncogene.* 22:8568–8580.

Mallart, A., D. Angaut-Petit, C. Bourret-Poulain, and A. Ferrus. 1991. Nerve terminal excitability and neuromuscular transmission in T(X;Y)V7 and Shaker mutants of *Drosophila melanogaster*. *J. Neurogenet.* 7:75–84.

Mercer, E.A., L. Korhonen, Y. Skoglosa, P.A. Olsson, J.P. Kukkonen, and D. Lindholm. 2000. NAIP interacts with hippocalcin and protects neurons against calcium-induced cell death through caspase-3-dependent and -independent pathways. *EMBO J.* 19:3597–3607.

Nabekura, J., T. Ueno, S. Katsurabayashi, A. Furuta, N. Akaike, and M. Okada. 2002a. Reduced NR2A expression and prolonged decay of NMDA receptor-mediated synaptic current in rat vagal motoneurons following axotomy. *J. Physiol.* 539:735–741.

Nabekura, J., T. Ueno, A. Okabe, A. Furuta, T. Iwaki, C. Shimizu-Okabe, A. Fukuda, and N. Akaike. 2002b. Reduction of KCC2 expression and GABAA receptor-mediated excitation after in vivo axonal injury. *J. Neurosci.* 22:4412–4417.

Nakamura, T.Y., D.J. Pountney, A. Ozaita, S. Nandi, S. Ueda, B. Rudy, and W.A. Coetzee. 2001. A role for frequenin, a Ca^{2+}-binding protein, as a regulator of Kv4 K^+-currents. *Proc. Natl. Acad. Sci. USA.* 98:12808–12813.

Nakamura, T.Y., E. Sturm, D.J. Pountney, B. Orenzoff, M. Artman, and W.A. Coetzee. 2003. Developmental expression of NCS-1 (frequenin), a regulator of Kv4 K^+ channels, in mouse heart. *Pediatr. Res.* 53:554–557.

Nicole, O., C. Ali, F. Docagne, L. Plawinski, E.T. MacKenzie, D. Vivien, and A. Buisson. 2001. Neuroprotection mediated by glial cell line-derived neurotrophic factor: involvement of a reduction of NMDA-induced calcium influx by the mitogen-activated protein kinase pathway. *J. Neurosci.* 21:3024–3033.

Olafsson, P., T. Wang, and B. Lu. 1995. Molecular cloning and functional characterization of the *Xenopus* Ca^{2+}-binding protein frequenin. *Proc. Natl. Acad. Sci. USA.* 92:8001–8005.

Oppenheim, R.W., L.J. Houenou, J.E. Johnson, L.F. Lin, L. Li, A.C. Lo, A.L. Newsome, D.M. Prevette, and S. Wang. 1995. Developing motor neurons rescued from programmed and axotomy-induced cell death by GDNF. *Nature.* 373:344–346.

Perez-Garcia, M.J., V. Cena, Y. de Pablo, M. Llovera, J.X. Comella, and R.M. Soler. 2004. Glial cell line-derived neurotrophic factor increases intracellular calcium concentration. Role of calcium/calmodulin in the activation of the phosphatidylinositol 3-kinase pathway. *J. Biol. Chem.* 279:6132–6142.

Perrelet, D., A. Ferri, P. Liston, P. Muzzin, R.G. Korneluk, and A.C. Kato. 2002. IAPs are essential for GDNF-mediated neuroprotective effects in injured motor neurons in vivo. *Nat. Cell Biol.* 4:175–179.

Pongs, O., J. Lindemeier, X.R. Zhu, T. Theil, D. Engelkamp, I. Krah-Jentgens, H.G. Lambrecht, K.W. Koch, J. Schwemer, R. Rivosecchi, et al. 1993. Frequenin–a novel calcium-binding protein that modulates synaptic efficacy in the *Drosophila* nervous system. *Neuron.* 11:15–28.

Rothstein, J.D., S. Patel, M.R. Regan, C. Haenggeli, Y.H. Huang, D.E. Bergles, L. Jin, M. Dykes Hoberg, S. Vidensky, D.S. Chung, et al. 2005. Beta-lactam antibiotics offer neuroprotection by increasing glutamate transporter expression. *Nature.* 433:73–77.

Sippy, T., A. Cruz-Martin, A. Jeromin, and F.E. Schweizer. 2003. Acute changes in short-term plasticity at synapses with elevated levels of neuronal calcium sensor-1. *Nat. Neurosci.* 6:1031–1038.

Soler, R.M., X. Dolcet, M. Encinas, J. Egea, J.R. Bayascas, and J.X. Comella. 1999. Receptors of the glial cell line-derived neurotrophic factor family of neurotrophic factors signal cell survival through the phosphatidylinositol 3-kinase pathway in spinal cord motoneurons. *J. Neurosci.* 19:9160–9169.

Takahashi, M. 2001. The GDNF/RET signaling pathway and human diseases. *Cytokine Growth Factor Rev.* 12:361–373.

Tsujimoto, T., A. Jeromin, N. Saitoh, J.C. Roder, and T. Takahashi. 2002. Neuronal calcium sensor 1 and activity-dependent facilitation of P/Q-type calcium currents at presynaptic nerve terminals. *Science.* 295:2276–2279.

Wang, C.Y., F. Yang, X. He, A. Chow, J. Du, J.T. Russell, and B. Lu. 2001. Ca^{2+} binding protein frequenin mediates GDNF-induced potentiation of Ca^{2+} channels and transmitter release. *Neuron.* 32:99–112.

Wang, Y., C.F. Chang, M. Morales, Y.H. Chiang, and J. Hoffer. 2002. Protective effects of glial cell line-derived neurotrophic factor in ischemic brain injury. *Ann. NY Acad. Sci.* 962:423–437.

Weiss, J.L., D.A. Archer, and R.D. Burgoyne. 2000. Neuronal Ca^{2+} sensor-1/frequenin functions in an autocrine pathway regulating Ca^{2+} channels in bovine adrenal chromaffin cells. *J. Biol. Chem.* 275:40082–40087.

Weisz, O.A., G.A. Gibson, S.M. Leung, J. Roder, and A. Jeromin. 2000. Overexpression of frequenin, a modulator of phosphatidylinositol 4-kinase, inhibits biosynthetic delivery of an apical protein in polarized madin-darby canine kidney cells. *J. Biol. Chem.* 275:24341–24347.

Yamamoto, M., N. Mitsuma, Y. Ito, N. Hattori, M. Nagamatsu, M. Li, T. Mitsuma, and G. Sobue. 1998. Expression of glial cell line-derived neurotrophic factor and GDNFR-alpha mRNAs in human peripheral neuropathies. *Brain Res.* 809:175–181.

Yan, Q., C. Matheson, and O.T. Lopez. 1995. In vivo neurotrophic effects of GDNF on neonatal and adult facial motor neurons. *Nature.* 373:341–344.

Growth was assayed by measuring the reduction of sodium 2,3-bis-[2-methoxy-4-nitro-5-sulfophenyl]-2*H*-tetrazolium-5-carboxanilide (XTT) [11]. Amphotericin-B was used as positive control [12], and the cell toxicity was assessed by measuring the reduction of XTT by murine macrophages (cell line J744) and VERO cells [13], [14].

Acknowledgements

This work was supported by US NIH grant #1U01 TW00663401 from the International Cooperative Biodiversity Groups Program ICBG-Panama and by funds from the Smithsonian Tropical Research Institute.

References

[1] Montenegro H, Gutiérrez M, Romero LI, Ortega-Barría , Capson TL, Cubilla L. Aporphine alkaloids from *Guatteria* spp. with leishmanicidal activity. Planta Med 2003; 69: 677–9

[2] Berman J. Recent developments in leishmaniasis: epidemiology, diagnosis, and treatment. Curr Infect Dis Rep 2005; 7: 33–8

[3] Li D, Zhao B, Sim SP, Li TK, Liu A, Liu LF et al. 2,3-Dimethoxybenzo[*i*]phenanthridines: topoisomerase I-targeting anticancer agents. Bioorg Med Chem 2003; 11: 521–8

[4] Iwasa K, Nishiyama Y, Ichimaru M, Moriyasu M, Kim HS, Wataya Y et al. Structure-activity relationships of quaternary protoberberine alkaloids having an antimalarial activity. Eur J Med Chem 1999; 34: 1077–83

[5] Werbovetz A, Bhattacharjee K, Brendle J, Scovil P. Analysis of stereoelectronic properties of camptothecin analogues in relation to biological activity. Bioorg Med Chem 2000; 8: 1741–7

[6] Guinaudeau H, Leboeuf M, Cave A. Aporphine alkaloids. J Nat Prod 1975; 38: 275–335

[7] Hocquemiller R, Cave A, Raharisololalao A. Alcaloides de *Xylopya buxifolia* et de *Xylopia danguyella*. J Nat Prod 1981; 44: 551–6

[8] Chen CL, Chang HM, Cowling E, Huang CY, Gates R. Aporphine alkaloids and lignans formed in response to injury of sapwood in *Liriodendron tulipifera*. Phytochemistry 1976; 15: 1161–7

[9] Castro O, López J, Vergara A. Aporphine alkaloids from *Phoebe pittieri*. Phytochemistry 1985; 24: 203–4

[10] Gellert E, Summons RE. Alkaloids of the genus *Cinnamomum*. II. Alkaloids of the bark of *Cinnamomum* sp. T.G.H. 13077. Aust J Chem 1970; 23: 2095–9

[11] Williams C, Espinosa OA, Montenegro H, Cubilla L, Capson TL, Ortega-Barría E et al. Hydrosoluble formazan XTT: its application to natural products drug discovery for *Leishmania*. J Microbiol Methods 2003; 55: 813–6

[12] Golenser J, Frankenburg S, Enrenfreund T, Domb AJ. Efficacious treatment of experimental leishmaniasis with amphotericin B-arabinogalactan water-soluble derivatives. Antimicrob Agents Chemother 1999; 43: 2209–14

[13] Shin IS, Tanifuji H, Arata Y, Morizawa Y, Nakayama T, Wataya Y. 3′-Deoxy-3′-fluoroinosine as a potent antileishmanial agent. The metabolism and selective cytotoxic effect of 3′-deoxy-3′-fluoroinosine against *Leishmania tropica* and *L. donovani in vitro* and *in vivo*. Parasitol Res 1995; 81: 622–6

[14] Sahpaz S, Bories C, Loiseau PM, Cortes D, Hocquemiller R, Laurens A et al. Cytotoxic and antiparasitic activity from *Annona senegalensis* seeds. Planta Med 1994; 60: 538–40

Inhibitory Effects of Ginsenoside-Rb1 on Activation of the 12-*O*-Tetradecanoylphorbol 13-Acetate-Induced Cyclooxygenase-2 Promoter

Wankyu Park[1], Wonchung Lim[1], Jungyoon Cho[1], Hiroyasu Inoue[2], Mee-Ra Rhyu[3], YoungJoo Lee[1]

Abstract

We studied the inhibitory effects of ginsenoside-Rb1 (**1**) on 12-*O*-tetradecanoylphorbol 13-acetate (TPA)-induced transcriptional activation of the cyclooxygenase-2 (COX-2) promoter. The suppressive activity of ginsenoside-Rb1 was characterized using COX-2 promoter-driven luciferase reporter plasmids in a transient transfection system. Ginsenoside-Rb1 at 100 μM inhibited TPA-induced transcriptional activation of the COX-2 promoter. To identify the *cis*-acting elements responsible for this inhibition, the effects of site-specific mutations in the COX-2 promoter region were examined. Inhibition by ginsenoside-Rb1 was not affected by mutations in nuclear factor-κB- or cAMP-responsive elements. However, the effects were abolished when the nuclear factor-interleukin-6 binding site was mutated, indicating that ginsenoside-Rb1 exerts its effects via this element. In conclusion, ginsenoside-Rb1 inhibits TPA-induced COX-2 promoter activity through the nuclear factor interleukin-6 binding site and not through the nuclear factor-κB or cAMP-responsive elements.

Ginseng has been used for thousands of years in Asian countries for its wide spectrum of medicinal properties. It has antioxidant, immunomodulatory, antiaging, and anticancer activities [1]. Use of ginseng has expanded to Western countries, and continues to rise with the increasing popularity of complementary and alternative medicine. Although the beneficial effects of ginseng have prompted tremendous efforts to discover the pharmacology of its action through biochemical and molecular biology techniques, a detailed mechanism has yet to be determined.

A number of ginseng components have been isolated and characterized, such as ginsenosides, polysaccharides, peptides, polyacetylenic alcohols, and fatty acids [2]. The major pharmacologically active components of ginseng are the ginsenosides, which are steroidal saponins comprising 3–6% of the total ginseng

Affiliation: [1] College of Life Science, Institute of Biotechnology, Department of Bioscience and Biotechnology, Sejong University, Seoul, Korea · [2] Department of Food Science and Nutrition, Faculty of Human Life and Environment, Nara Women's University, Nara, Japan · [3] Food Function Research Division, Korea Food Research Institute, Gyeonggi-Do, Korea

Correspondence: YoungJoo Lee, Ph. D. · Department of Bioscience and Biotechnology · Sejong University · Kwang-Jin-Gu · Seoul 143–747 · Korea · Phone: +82-2-3408-3766 · Fax: +82-2-3408-3334 · E-mail: yjlee@sejong.ac.kr

Received: January 14, 2005 · **Accepted:** August 3, 2005

Bibliography: Planta Med 2006; 72: 272–275 © Georg Thieme Verlag KG Stuttgart · New York · DOI 10.1055/s-2005-873172 · Published online November 10, 2005 · ISSN 0032-0943

mass [3]. In particular, ginseng extracts contain 0.4–1.8% ginsenoside-Rb1 (**1**; Fig. 1) by weight, depending on manufacturing and processing methods, which belongs to the protopanaxadiol class of ginsenosides [4]. Studies on the activity of ginsenoside-Rb1 have demonstrated effects on cardiac contraction, adrenal hydroxylase upregulation, and estrogenicity [5], [6], [7], [8].

Cyclooxygenase (prostaglandin H synthase; COX) is a key regulatory enzyme in the conversion of arachidonic acid to prostaglandins. It is found as two distinct isoforms: COX-1 is expressed constitutively in most tissues and COX-2 is inducible by extracellular stimuli such as tumor promoters, proinflammatory cytokines and growth factors [9], [10]. Several studies have indicated that induction of COX-2 expression is important in inflammation, immune responsivity, and carcinogenesis [11], [12]. Transcriptional activation of COX-2 is regulated by the binding of transcription factors to the COX-2 promoter, which contains multiple putative *cis*-acting elements for transcription factors. These elements include a cAMP-responsive element (CRE), an E-box, binding sites for nuclear factor (NF)-κB, NF-interleukin-6 (NF-IL6), and activator protein 2 (AP2). The consensus *cis*-acting sites of NF-kB, NF-IL6, and CRE are of major importance in hormone-, cytokine-, and tumor promoter-stimulated responses [13], [14], [15].

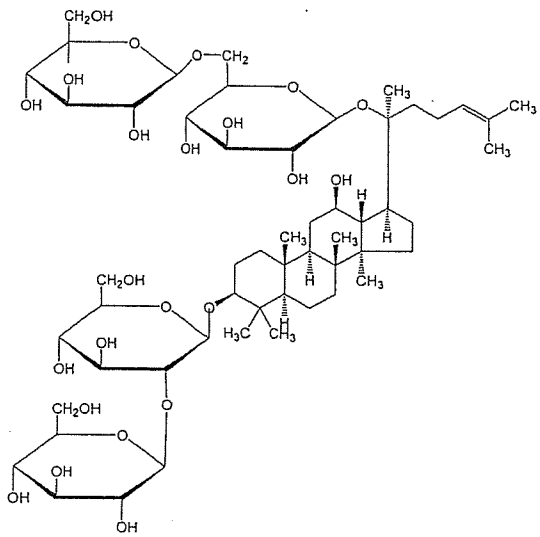

Fig. 1 The structure of ginsenoside-Rb1 (**1**).

In the present study, we examined the inhibition of 12-*O*-tetradecanoylphorbol 13-acetate (TPA)-induced COX-2 promoter activation by ginsenoside-Rb1, as well as the specific promoter binding sites involved in this process. The data, which were obtained using a COX-2 promoter-reporter system, demonstrate that ginsenoside-Rb1 has an inhibitory effect on the transcriptional activity of the TPA-induced COX-2 promoter, and that this inhibition is mediated through the NF-IL6 element.

A luciferase reporter gene under control of the full-length mouse COX-2 promoter was transiently transfected into COS cells, and the cells were exposed to 10 nM TPA with or without ginsenoside-Rb1 for 24 h. Treatment of cells with ginsenoside-Rb1 alone had no effect on luciferase activity driven by the COX-2 promoter. However, simultaneous treatment with TPA and ginsenoside-Rb1 decreased luciferase activity as compared to cells treated with TPA alone in a concentration-dependent manner (Figs. **2A** and **B**). These results suggest that ginsenoside-Rb1 inhibits TPA-induced COX-2 promoter activation. It is well known that another tumor promoter such as tumor necrosis factor α (TNFα) induces COX-2 [16]. As shown in Fig. **2C**, ginsenoside-Rb1 also inhibits TNFα-induced COX-2 promoter activation.

The 5′-flanking region of the COX-2 promoter (–327/+59) contains an NF-κB binding site (–223/–214), an NF-IL6 binding site (–132/–124), and a CRE (–59/–53) binding site [17]. To identify the region(s) involved in ginsenoside-Rb1-mediated COX-2 promoter inhibition, we transiently transfected reporter constructs containing mutations in either the NF-κB (KBM) or both the NF-IL6 and CRE (ILM/CRM) sites into COS cells. As shown in Fig. **3A**, the inhibitory effects of ginsenoside-Rb1 on TPA-induced COX-2 promoter activity were retained in cells transfected with the KBM reporter gene, indicating that NF-κB is not involved in ginsenoside-Rb1-mediated inhibition of COX-2 promoter activity. In contrast, ginsenoside-Rb1 had no inhibitory effect in cells transfected with the ILM/CRM reporter genes (Fig. **3B**). Furthermore, mutations in the NF-IL6 site (–132/–124) abolished ginsenoside-Rb1-mediated inhibition as compared to the effects on the full-length mouse COX-2 promoter (Fig. **4A**). These results suggest that ginsenoside-Rb1 exerts its inhibitory effects on COX-2 promoter activity via the NF-IL6 site. The relative lack of importance of the CRE and NF-κB sites in eliciting the ginsenoside-Rb1-mediated response was confirmed by experiments in which

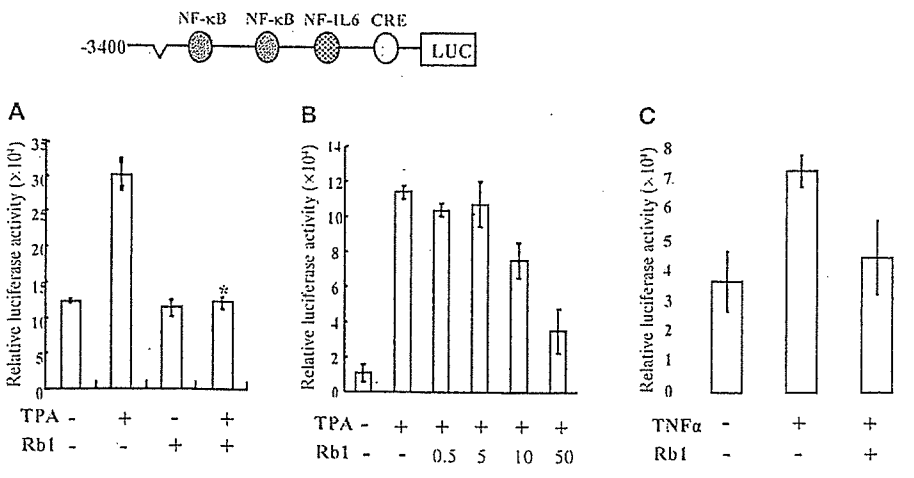

Fig. 2 Ginsenoside-Rb1 inhibits TPA-induced COX-2 promoter transcription activity. Cells were transiently transfected with the full length 3.4 kb COX-2 promoter and treated with 10 nM TPA and 100 μM of ginsenoside-Rb1 (A), 10 nM TPA with increasing concentrations of ginsenoside-Rb1 (B), or 10 ng/mL TNFα with ginsenoside-Rb1 (C) as indicated for 24 h, then assayed for luciferase activity as described in Materials and Methods. Transfections were performed in triplicate. One representative result is shown in this figure. Data are expressed as the mean ± S.E.M.

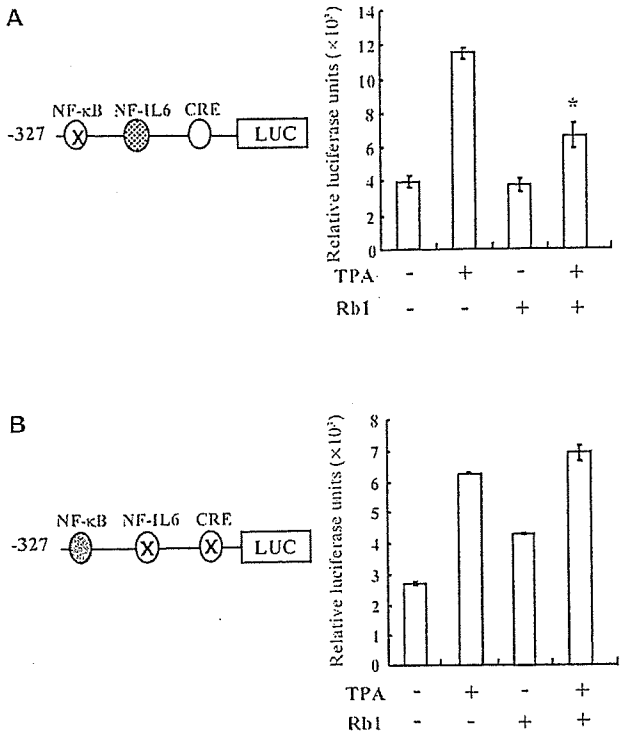

Fig. 3 NF-κB is not involved in ginsenoside-Rb1-mediated inhibition on TPA-induced COX-2 promoter activity. Cells were transiently transfected with KBM (A) or ILM/CRM (B) reporter gene, treated with 10 nM TPA and 100 μM ginsenoside-Rb1, and assayed for luciferase activity after 24 h of treatment. Data are representative of least three independent experiments performed in triplicate.

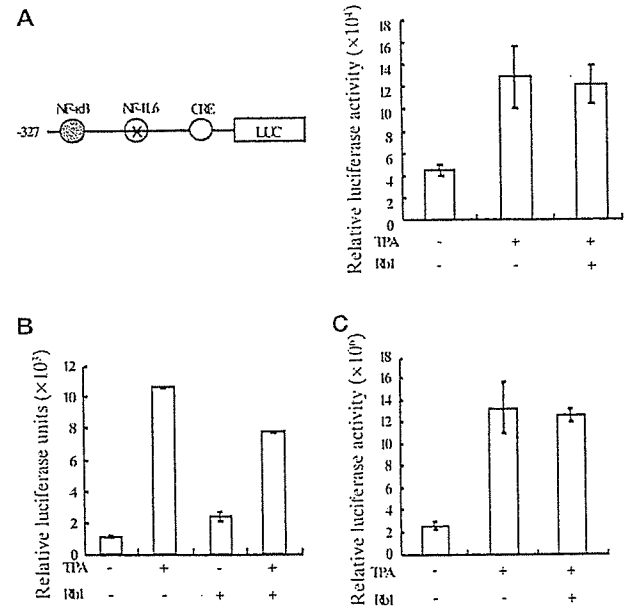

Fig. 4 The NF-IL6 site is responsible for ginsenoside-Rb1-mediated inhibition on TPA-induced COX-2 promoter activity. Cells were transiently transfected with ILM (A), or $p(CRE)_5$ (B), or $p(NF\text{-}\kappa B)_7$ (C) reporter gene and treated with of 10 nM TPA and 100 μM ginsenoside-Rb1 for 24 h. Transfections were performed in triplicate more than three times, and one representative dataset is shown.

COS cells were transiently transfected with $p(CRE)_5$-Luc or $p(NF\text{-}\kappa B)_7$-Luc constructs. As shown in Figs. 4B and C, ginsenoside-Rb1 had no significant effect on these cells.

In this study, we examined the effects of ginsenoside-Rb1 on TPA-induced COX-2 promoter activation. In particular, we attempted to identify the COX-2 promoter region that is important for mediating the inhibitory effects of ginsenoside-Rb1 by mutagenizing specific transcription factor binding sites in the COX-2 promoter. Our data indicate that ginsenoside-Rb1 inhibits TPA-induced COX-2 promoter stimulation via the NF-IL6 binding site. NF-IL6 is a pleiotropic transcription factor for numerous genes of cellular differentiation and inflammation such as IL-6, TNF-α, granulocyte colony stimulating factor, COX-2 and inducible nitric oxide synthase [18]. It has been shown that COX-2 expression is regulated through NF-IL6 by staurosporin, sauchinone from *Saurus chinensis*, and aspirin [14], [15], [19]. In addition, NF-IL6 is one of the targets for the COX-2 regulation in many cancer cells [20]. Our results on the effects of ginsenoside-Rb1 on COX-2 implicate the clinical value of ginseng for the treatment of inflammation and tumor growth and provide a mechanistic clue to the antitumor activity of ginseng, although the exact nature of the activity is far from clear. Future studies investigating the effects of ginsenoside-Rb1 on endogenous COX-2 gene expression in various cancer cell lines and in *in vitro* tumor models will be helpful in further elucidating the molecular mechanism of ginsenoside-Rb1-mediated inhibition of TPA-induced COX-2 promoter activation.

Materials and Methods

Ginsenoside-Rb1, provided by the Korea Ginseng and Tobacco Research Institute (Daejeon, Korea), was dissolved in 20% ethanol at a concentration of 15 mg/mL and added to the medium at 100 μM. An untreated group served as a control. TPA and TNFα were obtained from Sigma and used at 10 nM and 10 ng/mL, respectively.

The mouse COX-2 full promoter luciferase reporter construct was kindly provided by Dr. Hui-Fang Cheng. The human COX-2 promoter driven mutated constructs were cloned as described [17]. The plasmids $p(CRE)_4$-Luc and $p(NF\text{-}\kappa B)_5$-Luc were purchased from Stratagene.

COS cells, a monkey kidney cell line, were maintained in phenol red-free Dulbecco's modified Eagle's medium from Sigma (DMEM) with 10% (vol/vol) calf serum (GIBCO).

Cells were transiently transfected by electroporation as described [21]. Electroporation was performed with a Gene Pulser II (Bio-Rad). Cells were trypsinized, washed in cold PBS, and resuspended in PBS. A 400-μL portion of the suspension was mixed with 20 μg of plasmid DNA. After 5 min at room temperature, cells were pulsed at 1000 μF and 250 V. After 10 min incubation at 37 °C, the suspension was diluted in medium and cultured for 24 h. Cells were replaced with fresh medium and treated for 24 h. After treatment, the cells were harvested and lysed with reporter lysis buffer (Promega Luciferase Assay system). The cell extract was mixed with the luciferase assay reagent, analyzed by the AutoLumat LB953 luminometer and expressed as relative light units. The mean and standard errors of triplicate or quadruplicate samples are shown for representative experiments. All transfection experiments were repeated three or more times with similar results.

Values shown represent mean ± SEM. Statistical analysis was performed by Student's *t* test with a *p* value of less than 0.05 being considered statistically significant.

Acknowledgements

This work was supported in part by grants from the Korea Tobacco and Ginseng Corp. R&D program 2002, Korean Ministry of Health and Welfare (HMP-00-0-21600-009), and BK21 program to Y. J. Lee.

References

[1] Attele AS, Wu JA, Yuan CS. Ginseng pharmacology: multiple constituents and multiple actions. Biochem Pharmacol 1999; 58: 1685–93

[2] Liu WK, Xu SX, Che CT. Anti-proliferative effect of ginseng saponins on human prostate cancer cell line. Life Sci 2000; 67: 1297–306

[3] Yoon M, Lee H, Jeong S, Kim JJ, Nicol CJ, Nam KW et al. Peroxisome proliferator-activated receptor alpha is involved in the regulation of lipid metabolism by ginseng. Br J Pharmacol 2003; 138: 1295–302

[4] Shibata S. Chemistry and cancer preventing activities of ginseng saponins and some related triterpenoid compounds. J Korean Med Sci 2001; 16 (Suppl): S28S37

[5] Morschl E, Bretus I, Nemcsik J, Laszlo F, Pavo I. Estrogen-mediated upregulation of the Ca-dependent constitutive nitric oxide synthase in the rat aorta and heart. Life Sci 2000; 68: 49–55

[6] Scott GI, Colligan PB, Ren BH, Ren J. Ginsenosides Rb1 and Re decrease cardiac contraction in adult rat ventricular myocytes: role of nitric oxide. Br J Pharmacol 2001; 134: 1159–65

[7] Kim HS, Zhang YH, Fang LH, Lee MK. Effects of ginsenosides on bovine adrenal tyrosine hydroxylase. J Ethnopharmacol 1999; 66: 107–11

[8] Cho JY, Park WK, Lee SG, Ahn WS, Lee YJ. Ginsenoside-Rb1 from *Panax ginseng* C.A. Meyer activates estrogen receptor-alpha and -beta, independent of ligand binding. J Clin Endocrinol Metab 2004; 89: 3510–5

[9] Funk CD, Funk LB, Kennedy ME, Pong AS, Fitzgerald GA. Human platelet/erythroleukemia cell prostaglandin G/H synthase: cDNA cloning, expression, and gene chromosomal assignment. FASEB J 1991; 5: 2304–12

[10] Smith WL, DeWitt DL, Garavito RM. Cyclooxygenases: structural, cellular, and molecular biology. Annu Rev Biochem 2000; 69: 45–82

[11] Chen CC, Sun YT, Chen JJ, Chiu KT. TNF-alpha-induced cyclooxygenase-2 expression in human lung epithelial cells: involvement of the phospholipase C-gamma 2, protein kinase C-alpha, tyrosine kinase, NF-kappa B-inducing kinase, and I-kappa B kinase 1/2 pathway. J Immunol 2000; 165: 2719–28

[12] Chen Y, Yang L, Lee TJ. Oroxylin A inhibition of lipopolysaccharide-induced iNOS and COX-2 gene expression via suppression of nuclear factor-kappaB activation. Biochem Pharmacol 2000; 59: 1445–57

[13] Sirois J, Levy LO, Simmons DL, Richards JS. Characterization and hormonal regulation of the promoter of the rat prostaglandin endoperoxide synthase 2 gene in granulosa cells. Identification of functional and protein-binding regions. J Biol Chem 1993; 268: 12199–206

[14] Saunders MA, Sansores-Garcia L, Gilroy DW, Wu KK. Selective suppression of CCAAT/enhancer-binding protein beta binding and cyclooxygenase-2 promoter activity by sodium salicylate in quiescent human fibroblasts. J Biol Chem 2001; 276: 18897–904

[15] Wang CY, Lei HJ, Huang CY, Zhang Z, Mukherjee AB, Yuan CJ. Induction of cyclooxygenase-2 by staurosporine through the activation of nuclear factor for IL-6 (NF-IL6) and activator protein 2 (AP2) in an osteoblast-like cell line. Biochem Pharmacol 2002; 64: 177–84

[16] Yamamoto K, Arakawa T, Ueda N, Yamamoto S. Transcriptional roles of nuclear factor κB and nuclear factor-interleukin-6 in the tumor necrosis factor α-dependent induction of cyclooxygenase-2 in MC3T3-E1 cells. J Biol Chem 1995; 270: 31315–20

[17] Inoue H, Umesono K, Nishimori T, Hirata Y, Tanabe T. Glucocorticoid-mediated suppression of the promoter activity of the cyclooxygenase-2 gene is modulated by expression of its receptor in vascular endothelial cells. Biochem Biophys Res Commun 1999; 254: 292–8

[18] Hattori T, Ohoka N, Hayashi H, Onozaki K. C/EBP homologous protein (CHOP) up-regulates IL-6 transcription by trapping negative regulating NF-IL6 isoform. FEBS Lett 2003; 541: 33–9

[19] Lee AK, Sung SH, Kim YC, Kim SG. Inhibition of lipopolysaccharide-inducible nitric oxide synthase, TNF-α and COX-2 expression by sauchinone effects on I-κBa phosphorylation, C/EBP and AP-1 activation. Br J Pharmacol 2003; 139: 11–20

[20] Wardlaw SA, Zhang N, Belinsky SA. Transcriptional regulation of basal cyclooxygenase-2 expression in murine lung tumor-derived cell lines by CCAAT/enhancer-binding protein and activating transcription factor/cAMP response element-binding protein. Mol Pharmacol 2002; 62: 326–33

[21] Faussner A, Bauer A, Kalatskaya I, Jochum M, Fritz H. Expression levels strongly affect ligand-induced sequestration of B2 bradykinin receptors in transfected cells. Am J Physiol Heart Circ Physiol 2003; 284: 1892–8

Acta Crystallographica Section F
Structural Biology and Crystallization Communications
ISSN 1744-3091

Crystallization and preliminary X-ray crystallographic analysis of two vascular apoptosis-inducing proteins (VAPs) from *Crotalus atrox* venom

Tomoko Igarashi,[a] Yuko Oishi,[a] Satohiko Araki,[b] Hidezo Mori[a] and Soichi Takeda[a,c]*

[a]Department of Cardiac Physiology, National Cardiovascular Center Research Institute, 5-7-1 Fujishiro-dai, Suita, Osaka 565-8565, Japan, [b]Sugashima Marine Biological Laboratory, Graduate School of Science, Nagoya University, Toba, Mie 517-0004, Japan, and [c]Laboratory for Structural Biochemistry, Riken Harima Institute at SPring-8, 1-1-1 Kouto, Mikazuki, Sayo, Hyogo 679-5148, Japan

Correspondence e-mail: stakeda@ri.ncvc.go.jp

Received 11 May 2006
Accepted 12 June 2006

VAPs are haemorrhagic snake-venom toxins belonging to the reprolysin family of zinc metalloproteinases. *In vitro*, VAPs induce apoptosis specifically in cultured vascular endothelial cells. VAPs have a modular structure that bears structural homology to mammalian ADAMs (a disintegrin and metalloproteinases). VAP1 is a homodimer with a MW of 110 kDa in which the monomers are connected by a single disulfide bridge. VAP2 is homologous to VAP1 and exists as a monomer with a MW of 55 kDa. In the current study, several crystal forms of VAP1 and VAP2 were obtained using the vapour-diffusion method and diffraction data sets were collected using SPring-8 beamlines. The best crystals of VAP1 and VAP2 generated data sets to 2.5 and 2.15 Å resolution, respectively.

1. Introduction

Haemorrhagic snake venoms contain factors that induce apoptosis specifically in cultured vascular endothelial cells (Araki *et al.*, 1993). The vascular apoptosis-inducing proteins VAP1 and VAP2 were originally isolated from the venom of the western diamondback rattlesnake *Crotalus atrox* (Masuda *et al.*, 1997, 1998) and similar apoptotic toxins (VAPs) have been isolated from other snake venoms (Masuda *et al.*, 2001; You *et al.*, 2003; Trummal *et al.*, 2005). VAP1 is a disulfide-bonded homodimeric protein with a molecular weight of 110 kDa and an isoelectric point of 8.5. VAP2 is an acidic single-chain protein with a molecular weight of 55 kDa and an isoelectric point of 4.5 (Masuda *et al.*, 1997, 1998). VAP1 (Masuda *et al.*, 2000) and VAP2 (S. Masuda, H. Hayashi & S. Araki, in preparation) are modular metalloproteinases with nucleotide-sequence homology to genes encoding the mammalian membrane-anchored metalloproteinases known as ADAMs. ADAMs are an emerging class of metalloproteinases whose function has been implicated in cell–cell and cell–matrix adhesion and signalling. They also appear to be associated with numerous diseases including arthritis, Alzheimer's disease and cancer (White, 2003; Blobel, 2005; Seals & Courtneidge, 2003; Moss & Bartsch, 2004; Duffy *et al.*, 2003).

Viperidae snake venoms contain a number of metalloproteinases, the snake-venom metalloproteinases (SVMPs), that induce local and systemic haemorrhage by disrupting the wall of the blood vessels in envenomed patients (Gutierrez *et al.*, 2005). All known VAPs belong to the P-III class of SVMPs, which have been shown to be the most potent haemorrhagic toxins from snake venoms. The P-III SVMPs have a modular structure consisting of metalloproteinase (M), disintegrin (D) and cysteine-rich (C) domains (Fox & Serrano, 2005). SVMPs and ADAMs are members of the reprolysin group of zinc-dependent metalloproteinases, which together with astasins, serralysin and matrix metalloproteinases comprise the metzincin superfamily of metalloproteinases (Bode *et al.*, 1993). All these enzymes share a signature consensus zinc-binding motif, HE*XX*H*XX*G*XX*H, in their catalytic region that defines proteins of the class, as well as a methionine-containing turn that serves as a structural base for the three active histidine residues (Bode *et al.*, 1993).

The crystal structures of several SVMPs of the P-I class, which contain only an M domain, and of isolated domains of ADAMs have

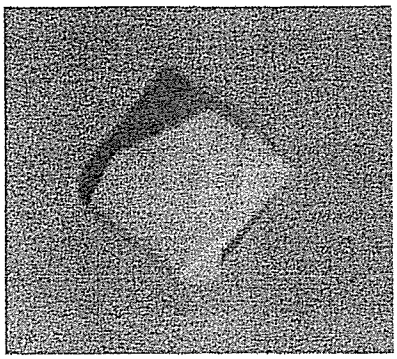

Table 1
Data-collection statistics for VAP1 crystals.

Values in parentheses are for the highest resolution shell. For each data set, a single crystal was used for measurement.

	Form 1-1	Form 1-2
Space group	$P4_12_12$	$P2_12_12_1$
Unit-cell parameters		
a (Å)	93.9	86.7
b (Å)	93.9	93.3
c (Å)	244.8	137.7
$\alpha = \beta = \gamma$ (°)	90	90
Beamline (detector)	BL45PX (Rigaku Jupiter)	BL45PX (Rigaku R-AXIS V)
Wavelength (Å)	0.98	1.0
Resolution (Å)	50–2.50 (2.59–2.50)	50–2.50 (2.59–2.50)
No. of unique reflections	38868 (3773)	38926 (3800)
R_{merge}†	0.084 (0.380)	0.072 (0.369)
$I/\sigma(I)$	18.7 (7.1)	14.4 (2.9)
Completeness (%)	99.7 (99.6)	99.4 (98.8)
Redundancy	12.7	3.91
No. of molecules in ASU	1	1
Matthews value (Å^3 Da^{-1})	2.5	2.5
Solvent content (%)	51	51

† $R_{merge} = \sum_{hkl} \sum_i |I_i(hkl) - \langle I(hkl)\rangle| / \sum_{hkl} \sum_i I_i(hkl)$, where $I_i(hkl)$ is the ith intensity measurement of reflection hkl and $\langle I(hkl)\rangle$ is its average.

been determined. However, structures of SVMPs or ADAMs containing M, D and C domains have not been determined. To understand more about the structure of P-III SVMPs and ADAMs and how it relates to the molecular mechanism of VAP-induced apoptosis, we initiated the crystallographic analysis of VAP1 and VAP2. This is the first report of the crystallization and preliminary X-ray analysis of apoptotic SVMPs. Three-dimensional crystal structures of VAP1 derived from the two distinct crystal forms described in this report have recently been described (Takeda *et al.*, 2006); the structural analysis of VAP2 is ongoing.

2. Methods

2.1. Purification

VAP1 and VAP2 were purified as described previously (Maruyama *et al.*, 2005; Masuda *et al.*, 1998) with some modifications. Briefly, crude *C. atrox* venom (Sigma–Aldrich, USA) was dissolved in buffer containing 10 m*M* Tris–HCl pH 7.0 and 10 m*M* NaCl and then applied onto a CM-Sepharose (Amersham Bioscience, USA) column equilibrated with the same buffer. VAP2 was eluted from the column with the above buffer, whereas VAP1 was eluted with buffer containing 10 m*M* Tris–HCl pH 7.0 and 50 m*M* NaCl.

The VAP1 was further purified on a hydroxylapatite column. The VAP1-containing CM-Sepharose fraction was first diluted with an equal amount of distilled water and then applied onto a hydroxylapatite column equilibrated with 25 m*M* sodium phosphate pH 7.0. VAP1 was eluted using buffer containing 50 m*M* sodium phosphate pH 7.0 and then concentrated using an Amicon Ultra membrane (Millipore) with a nominal molecular-weight limit (NMWL) of 50 000 Da. The final protein concentration was 6.5 mg ml^{-1}. During the concentration step, the buffer was replaced with 10 m*M* Tris–HCl pH 7.0.

The VAP2-containing CM-Sepharose fraction was loaded onto a Resource Q (GM Healthcare) column equilibrated with 10 m*M* Tris–HCl pH 8.0 and 50 m*M* NaCl and then eluted with a gradient of NaCl. 55 kDa molecular-weight fractions, which were eluted at about 130 m*M* NaCl, were pooled and concentrated by Amicon Ultra with a 30 000 NMWL membrane. The final protein concentration was 3.8 mg ml^{-1} in buffer containing 10 m*M* Tris–HCl pH 8.0.

2.2. Initial crystallization screen

Initial screening for appropriate crystallization conditions for VAP1 and VAP2 was carried out using the sitting-drop vapour-diffusion method and Crystal Screen (Hampton Research, USA), with or without 63 µg ml^{-1} (almost twice the molar protein concentration) of the hydroxyamate inhibitor 3-(*N*-hydroxycarboxamide)-2-isobutyl-propanoyl-Trp-methylamide (GM6001, Calbiochem) in the protein solution. A volume of 0.3–0.5 µl protein solution was mixed with an equal amount of reservoir solution and droplets were allowed to equilibrate against 0.1 ml reservoir solution at 293 K.

2.3. Diffraction data collection

Crystals were cryoprotected, mounted in a nylon loop (Hampton Research, USA) or in a Lytho Loop (Protein Wave Corp., Japan) and immediately exposed to a stream of nitrogen gas at 100 K to flash-freeze the samples. The preliminary X-ray data were collected using an in-house X-ray diffractometer (Rigaku Micromax-007 X-ray generator with R-AXIS VII imaging-plate detector) and crystals that diffracted well were selected for data acquisition using the beamlines at SPring-8. All diffraction data sets were collected using undulator beamlines (BL41XU, BL45XU) at 100 K and diffraction images were processed using the *HKL*2000 software (Otwinowski & Minor, 1997).

3. Results

3.1. VAP1 crystals

3.1.1. Crystallization. VAP1 was reproducibly crystallized in two distinct crystal forms. Crystals were initially obtained using Crystal

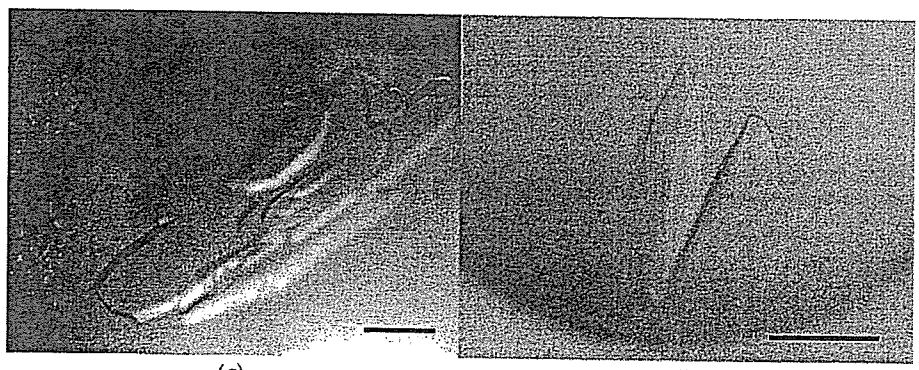

(*a*) (*b*)

Figure 1
VAP1 crystals. (*a*) Form 1-1. (*b*) Form 1-2. The scale bars indicate 0.1 mm.

Table 2
Data-collection statistics for VAP2 crystals.

Values in parentheses are for the highest resolution shell. For each data set, a single crystal was used for measurement.

	Form 2-1	Form 2-2	Form 2-3	Form 2-4	Form 2-5
GM6001	+	+	+	+	−
Space group	$P2_1$	$P2_12_12_1$	$P4_1$	$P6_322$	$C2$
Unit-cell parameters					
a (Å)	56.9	57.7	60.7	156.8	220.7
b (Å)	138.0	118.2	60.7	156.8	79.5
c (Å)	59.2	138.5	257.9	95.6	58.7
α (°)	90	90	90	90	90
β (°)	91.5	90	90	90	91.7
γ (°)	90	90	90	120	90
Beamline (detector)	BL41XU (ADSC Quantum 310R CCD detector)				
Wavelength (Å)	1.0	1.0	1.0	1.0	1.0
Resolution (Å)	50–2.15 (2.23–2.15)	50–2.50 (2.59–2.50)	50–3.20 (3.31–3.2)	50–3.80 (3.94–3.80)	50–2.70 (2.80–2.70)
No. of unique reflections	48664 (4428)	33288 (2925)	15097 (1437)	7169 (682)	26911 (2313)
R_{merge}†	0.081 (0.196)	0.089 (0.321)	0.091 (0.360)	0.117 (0.397)	0.085 (0.231)
$I/\sigma(I)$	9.8 (4.6)	10.3 (3.7)	10.9 (4.0)	8.4 (6.5)	10.1 (5.5)
Completeness (%)	98.1 (89.5)	98.6 (88.4)	99.5 (95.7)	99.8 (99.9)	95.9 (82.5)
Redundancy	3.3	6.5	7.0	19.2	3.4
No. of molecules in ASU	2	2	2	1	2
Matthews value (Å^3 Da^{-1})	2.4	2.4	2.5	3.1	2.7
Solvent content (%)	49	49	50	60	54

† $R_{merge} = \sum_{hkl}\sum_i |I_i(hkl) - \langle I(hkl)\rangle| / \sum_{hkl}\sum_i I_i(hkl)$, where $I_i(hkl)$ is the ith intensity measurement of reflection hkl and $\langle I(hkl)\rangle$ is its average.

Screen solution No. 46, but these crystals diffracted poorly. Subsequently, droplets were prepared by mixing 1 µl protein solution and 1 µl reservoir solution containing 15% PEG 8000, 0.1 *M* sodium cacodylate pH 6.5 and then equilibrated against 1 ml reservoir solution. Within a couple of weeks, using the hanging-drop method, improved tetragonal crystals (form 1-1; Fig. 1*a*) were obtained.

Orthorhombic crystals (form 1-2; Fig. 1*b*) were obtained using Additive Screen (Hampton Research, USA). The droplet was made by mixing 0.3 µl protein solution and 0.3 µl reservoir solution supplemented with one-fifth of the volume of 0.1 *M* cobalt(II) chloride (Additive Screen solution No. 4). The best crystals were obtained using the sitting-drop method after equilibration for 3 d against 0.1 ml of the same reservoir solution used to obtain form 1-1 crystals.

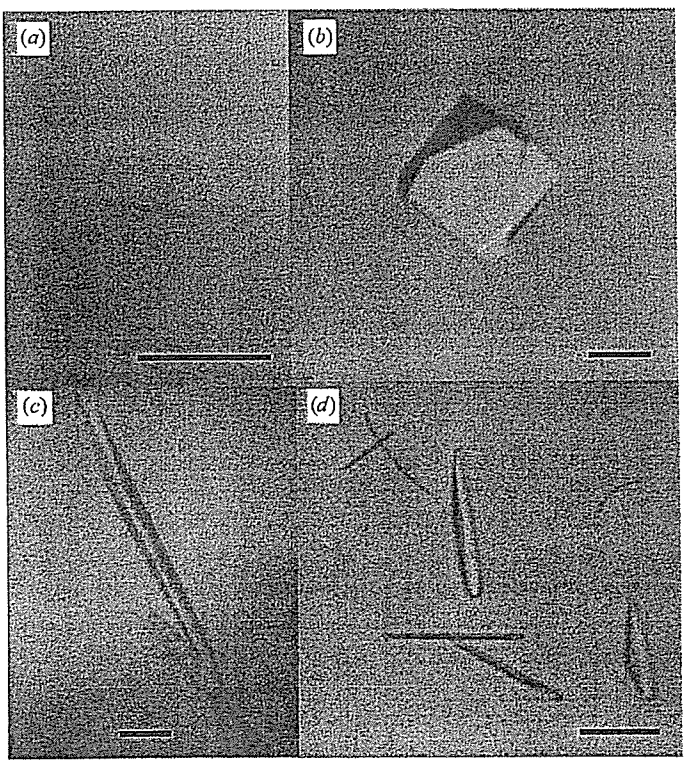

Figure 2
VAP2 crystals. (*a*) Form 2-2, (*b*) form 2-3, (*c*) form 2-4 and (*d*) form 2-5 crystals. The scale bars indicate 0.1 mm.

3.1.2. X-ray analysis. For X-ray measurements, crystals of either crystal form were soaked in a solution containing 15% PEG 8000, 5% methanol, 20% xylitol and 0.1 *M* sodium cacodylate pH 6.5 for cryoprotection prior to flash-freezing. X-ray diffraction data were obtained by the oscillation method using beamline BL45XU and an oscillation angle of 0.75° per image. Data sets were collected using a CCD detector (Rigaku Jupiter) for crystal form 1-1 or an imaging-plate detector (Rigaku R-AXIS V) for crystal form 1-2. The unit-cell parameters and the data statistics for the two crystal forms are summarized in Table 1. The structures were determined at 2.5 Å resolution by the molecular-replacement method using the P-I SVMP acutolysin-C (PDB code 1qua) as a starting model (Takeda *et al.*, 2006). The coordinates and the structure factors have been deposited in the PDB (2erq for form 1-1 and 2ero for form 1-2 crystals).

3.2. VAP2 crystals

3.2.1. Crystallization. Five distinct crystal forms of VAP2 were analyzed by X-ray diffraction. The initial screening for VAP2 crystals was performed in the presence and absence of the inhibitor GM6001.

In the presence of GM6001, Crystal Screen solution No. 10 yielded crystals. With this as a starting condition, the pH of the mother liquor, the PEG concentration and molecular weight and the species and concentrations of salts and additives were optimized and four distinct crystal forms were obtained (forms 2-1, 2-2, 2-3 and 2-4). These four forms were only obtained in the presence of GM6001 and were never obtained in its absence. Monoclinic (form 2-1) and orthorhombic (form 2-2; Fig. 2*a*) forms were obtained by the sitting-drop method under identical conditions as follows: droplets were made by mixing 0.5 µl protein solution with 0.5 µl reservoir solution containing 30% PEG 8000, 0.1 *M* ammonium acetate, 0.1 *M* sodium cacodylate pH 6.5 and were equilibrated against 0.1 ml reservoir solution. Tetragonal form crystals (form 2-3; Fig. 2*b*) were obtained by adding a one-tenth volume of 1 *M* potassium chloride (Additive Screen solution No. 16)

to the mother liquor and using a reservoir solution containing 30% PEG 8000, 0.1 *M* ammonium acetate, 0.1 *M* sodium acetate pH 4.6 with the same drop and reservoir volumes described above. Hexagonal crystals (form 2-4; Fig. 2*c*) were obtained by the hanging-drop method using 1 ml of a reservoir solution containing 20% PEG 20 000, 0.2 *M* calcium acetate, 0.1 *M* sodium cacodylate pH 6.5. The droplet was made by mixing 1 µl protein solution and 1 µl reservoir solution supplemented with a one-fifth volume of 0.3 *M* glycyl-glycyl-glycine solution (Additive Screen solution No. 34).

In the absence of GM6001, crystals were obtained with Crystal Screen solution No. 46, but these crystals yielded poor diffraction data. To improve the quality of the crystals, several additives were screened. Monoclinic crystals (form 2-5; Fig. 2*d*) were obtained by adding a one-tenth volume of 40% *n*-propanol solution (Additive Screen solution No. 90) to the reservoir solution (final composition 4% *n*-propanol, 16.2% PEG 8000, 0.18 *M* calcium acetate, 0.09 *M* sodium cacodylate pH 6.5). A mixture of 0.5 µl protein solution and 0.5 µl reservoir solution was equilibrated against 0.1 ml reservoir solution. These form 2-5 crystals were only obtained in the absence of GM6001 and were never obtained in its presence.

3.2.2. X-ray analysis. The mother liquors of the form 2-2 and 2-3 crystals were suitable for freezing; all others were first cryoprotected. For form 2-1 and 2-4 crystals, 20% glycerol was added to the reservoir solution for cryoprotection. For form 2-1, the cryogenic solution was added gradually to the crystal droplet in order to avoid cracking induced by osmotic shock. Crystal form 2-5 was rinsed in a solution containing 15% PEG 8000, 5% methanol, 20% xylitol and 0.1 *M* sodium cacodylate pH 6.5 and then immediately flash-frozen at 100 K. Because these crystals were extremely thin and fragile, they were mounted in a LithoLoop, an etched Mylar film, to prevent bending of the crystal.

All diffraction data sets for the VAP2 crystals were acquired using the oscillation method and beamline BL41XU (the oscillation angle was 1.0° for all data sets) at a wavelength of 1.0 Å and data were collected using an ADSC Quantum 310R detector. The unit-cell parameters and statistics for the data sets are summarized in Table 2. The estimated number of molecules in the asymmetric unit for each crystal form was obtained by a preliminary molecular-replacement method using *MOLREP* from the *CCP*4 suite (Collaborative Computational Project, Number 4, 1994) and the metalloproteinase (M) and cysteine-rich (C) domains of VAP1 (Takeda *et al.*, 2006) as the starting models. Structural analyses of these crystals along with the molecular-replacement phases are ongoing.

We thank Mariko Tomisako for her help in crystallization experiments and the staff of SPring-8 for assistance with data acquisition. This work was partly supported by Grant Nano-001 for Research on Advanced Medical Technology from the Ministry of Health, Labour and Welfare of Japan and by grants from the Takeda Science Foundation, from the Kao Foundation for Arts and Science and from the Senri Life Science Foundation.

References

Araki, S., Ishida, T., Yamamoto, T., Kaji, K. & Hayashi, H. (1993). *Biochem. Biophys. Res. Commun.* **190**, 148–153.
Blobel, C. P. (2005). *Nature Rev. Mol. Cell Biol.* **6**, 32–43.
Bode, W., Gomis-Ruth, F. X. & Stockler, W. (1993). *FEBS Lett.* **331**, 134–140.
Collaborative Computational Project, Number 4 (1994). *Acta Cryst.* D**50**, 760–763.
Duffy, M. J., Lynn, D. J., Lloyd, A. T. & O'Shea, C. M. (2003). *Thromb. Haemost.* **89**, 622–631.
Fox, J. W. & Serrano, S. M. (2005). *Toxicon*, **45**, 969–985.
Gutierrez, J. M., Rucavado, A., Escalante, T. & Diaz, C. (2005). *Toxicon*, **45**, 997–1011.
Maruyama, J., Hayashi, H., Miao, J., Sawada, H. & Araki, S. (2005). *Toxicon*, **46**, 1–6.
Masuda, S., Araki, S., Yamamoto, T., Kaji, K. & Hayashi, H. (1997). *Biochem. Biophys. Res. Commun.* **235**, 59–63.
Masuda, S., Hayashi, H. & Araki, S. (1998). *Eur. J. Biochem.* **253**, 36–41.
Masuda, S., Hayashi, H., Atoda, H., Morita, T. & Araki, S. (2001). *Eur. J. Biochem.* **268**, 3339–3345.
Masuda, S., Ohta, T., Kaji, K., Fox, J. W., Hayashi, H. & Araki, S. (2000). *Biochem. Biophys. Res. Commun.* **278**, 197–204.
Moss, M. L. & Bartsch, J. W. (2004). *Biochemistry*, **43**, 7227–7235.
Otwinowski, Z. & Minor, W. (1997). *Methods Enzymol.* **276**, 307–326.
Seals, D. F. & Courtneidge, S. A. (2003). *Genes Dev.* **17**, 7–30.
Takeda, S., Igarashi, T., Mori, H. & Araki, S. (2006). *EMBO J.* **25**, 2388–2396.
Trummal, K., Tonismagi, K., Siigur, E., Aaspollu, A., Lopp, A., Sillat, T., Saat, R., Kasak, L., Tammiste, I., Kogerman, P., Kalkkinen, N. & Siigur, J. (2005). *Toxicon*, **46**, 46–61.
White, J. M. (2003). *Curr. Opin. Cell Biol.* **15**, 598–606.
You, W. K., Seo, H. J., Chung, K. H. & Kim, D. S. (2003). *J. Biochem. (Tokyo)*, **134**, 739–749.

Available online at www.sciencedirect.com
ScienceDirect
Radiation Physics and Chemistry 75 (2006) 1841–1849
Radiation Physics and Chemistry
www.elsevier.com/locate/radphyschem

K-edge angiography utilizing a tungsten plasma X-ray generator in conjunction with gadolinium-based contrast media

Eiichi Sato[a,*], Yasuomi Hayasi[a], Etsuro Tanaka[b], Hidezo Mori[c], Toshiaki Kawai[d], Takashi Inoue[e], Akira Ogawa[e], Shigehiro Sato[f], Kazuyoshi Takayama[g], Jun Onagawa[h], Hideaki Ido[h]

[a]*Department of Physics, Iwate Medical University, 3-16-1 Honchodori, Morioka 020-0015, Japan*
[b]*Department of Nutritional Science, Faculty of Applied Bio-science, Tokyo University of Agriculture, 1-1-1 Sakuragaoka, Setagaya-ku 156-8502, Japan*
[c]*Department of Cardiac Physiology, National Cardiovascular Center Research Institute, 5-7-1 Fujishirodai, Suita, Osaka 565-8565, Japan*
[d]*Electron Tube Division #2, Hamamatsu Photonics K. K., 314-5 Shimokanzo, Iwata 438-0193, Japan*
[e]*Department of Neurosurgery, School of Medicine, Iwate Medical Universichimaru, Morioka 020-8505, Japan*
[f]*Department of Microbiology, School of Medicine, Iwate Medical University, 19-1 Uchimaru, Morioka 020-8505, Japan*
[g]*Shock Wave Research Center, Institute of Fluid Science, Tohoku University, 2-1-1 Katahira, Sendai 980-8577, Japan*
[h]*Department of Applied Physics and Informatics, Faculty of Engineering, Tohoku Gakuin University, 1-13-1 Chuo, Tagajo 985-8537, Japan*

Accepted 23 November 2005

Abstract

The tungsten plasma flash X-ray generator is useful in order to perform high-speed enhanced K-edge angiography using cone beams because K-series characteristic X-rays from the tungsten target are absorbed effectively by gadolinium-based contrast media. In the flash X-ray generator, a 150 nF condenser is charged up to 80 kV by a power supply, and flash X-rays are produced by the discharging. The X-ray tube is a demountable diode, and the turbomolecular pump evacuates air from the tube with a pressure of approximately 1 mPa. Since the electric circuit of the high-voltage pulse generator employs a cable transmission line, the high-voltage pulse generator produces twice the potential of the condenser charging voltage. At a charging voltage of 80 kV, the estimated maximum tube voltage and current were approximately 160 kV and 40 kA, respectively. When the charging voltage was increased, the characteristic X-ray intensities of tungsten K_α lines increased. The K_α lines were clean, and hardly any bremsstrahlung rays were detected. The X-ray pulse widths were approximately 110 ns, and the time-integrated X-ray intensity had a value of approximately 0.35 mGy at 1.0 m from the X-ray source with a charging voltage of 80 kV. Angiography was performed

*Corresponding author.
E-mail address: dresato@iwate-med.ac.jp (E. Sato).

0969-806X/$ - see front matter
doi:10.1016/j.radphyschem.2005.11.015